

# NAVAL POSTGRADUATE SCHOOL

## Monterey, California



# THESIS

AN ATMOSPHERIC GLOBAL PREDICTION  
MODEL USING A MODIFIED ARAKAWA  
DIFFERENCING SCHEME

by

Anthony Victor Monaco

March 1975

Thesis Advisor:

R. T. Williams

Approved for public release; distribution unlimited.

Thesis  
M6697

DUDLEY KNOX 11501  
NAVAL POSTGRADUATE SCHOOL  
MONTEREY, CALIFORNIA 93940

# NAVAL POSTGRADUATE SCHOOL

## Monterey, California



# THESIS

AN ATMOSPHERIC GLOBAL PREDICTION  
MODEL USING A MODIFIED ARAKAWA  
DIFFERENCING SCHEME

by

Anthony Victor Monaco

March 1975

Thesis Advisor:

R. T. Williams

Approved for public release; distribution unlimited.



REPORT DOCUMENTATION PAGE		READ INSTRUCTIONS BEFORE COMPLETING FORM
1. REPORT NUMBER	2. GOVT ACCESSION NO.	3. RECIPIENT'S CATALOG NUMBER
4. TITLE (and Subtitle) An Atmospheric Global Prediction Model Using a Modified Arakawa Differencing Scheme		5. TYPE OF REPORT & PERIOD COVERED Master's Thesis; March 1975
7. AUTHOR(s) Anthony Victor Monaco		6. PERFORMING ORG. REPORT NUMBER
9. PERFORMING ORGANIZATION NAME AND ADDRESS Naval Postgraduate School Monterey, California 93940		8. CONTRACT OR GRANT NUMBER(s)
11. CONTROLLING OFFICE NAME AND ADDRESS Naval Postgraduate School Monterey, California 93940		10. PROGRAM ELEMENT, PROJECT, TASK AREA & WORK UNIT NUMBERS
14. MONITORING AGENCY NAME & ADDRESS (if different from Controlling Office) Naval Postgraduate School Monterey, California 93940		12. REPORT DATE March 1975
		13. NUMBER OF PAGES 80
		15. SECURITY CLASS. (of this report) Unclassified
		15a. DECLASSIFICATION/DOWNGRADING SCHEDULE
16. DISTRIBUTION STATEMENT (of this Report) Approved for public release; distribution unlimited.		
17. DISTRIBUTION STATEMENT (of the abstract entered in Block 20, if different from Report)		
18. SUPPLEMENTARY NOTES		
19. KEY WORDS (Continue on reverse side if necessary and identify by block number) Atmospheric Global Prediction Model Modified Arakawa Differencing Scheme Analytic Initialization		
20. ABSTRACT (Continue on reverse side if necessary and identify by block number) A modified version of the new Arakawa differencing scheme for atmospheric global circulation was programmed for a two-level, adiabatic and frictionless model. In all cases analytic initial data were used to simplify evaluation. Experiments were designed to test various terms of the primitive equations as well as over-all performance.		



Block 20 - ABSTRACT (Cont.)

The 48-hour forecasts were well-behaved and showed good phase propagation.





An Atmospheric Global Prediction  
Model Using a Modified Arakawa  
Differencing Scheme

by

Anthony Victor Monaco  
Lieutenant, United States Navy  
B.S., United States Naval Academy, 1967

Submitted in partial fulfillment of the  
requirements for the degree of

MASTER OF SCIENCE IN METEOROLOGY

from the

NAVAL POSTGRADUATE SCHOOL  
March 1975

Thesis  
1867  
c. 2

## ABSTRACT

A modified version of the new Arakawa differencing scheme for atmospheric global circulation was programmed for a two-level, adiabatic and frictionless model. In all cases analytic initial data were used to simplify evaluation. Experiments were designed to test various terms of the primitive equations as well as over-all performance. The 48-hour forecasts were well-behaved and showed good phase propagation.



## TABLE OF CONTENTS

I.	INTRODUCTION -----	14
II.	MODEL DESCRIPTION -----	16
	A. VERTICAL COORDINATE SYSTEM -----	16
	B. PRIMITIVE EQUATIONS -----	18
	C. VERTICAL INDEX -----	20
	D. HORIZONTAL GRID AND DISTRIBUTION OF VARIABLES -----	22
	E. TIME DIFFERENCING -----	24
	F. AVERAGING THE PRESSURE GRADIENT AND ZONAL MASS FLUX NEAR THE POLES -----	26
	G. PROGRAM FORMAT -----	27
III.	FINITE DIFFERENCE EQUATIONS -----	30
	A. CONTINUITY EQUATION -----	30
	B. PRESSURE GRADIENT TERM AND THE HYDROSTATIC EQUATION -----	33
	1. Hydrostatic Equation -----	33
	2. $\eta$ -component of the Pressure Gradient Force -----	33
	3. $\xi$ -component of the Pressure Gradient Force -----	34
	C. MOMENTUM FLUXES -----	34
	D. CORIOLIS FORCE -----	36
	E. THERMODYNAMIC EQUATION -----	36
	F. POLAR MODIFICATION -----	37
	1. The Advective Terms in the $\xi$ -component of the Equation of Motion -----	38
	2. The Advective Terms in the $\eta$ -component of the Equation of Motion -----	42



IV. ANALYTIC INITIALIZATION ----- 44

    A. ANALYTIC BALANCING ----- 44

    B. ANALYTIC WINDS ----- 46

    C. TEMPERATURE ----- 46

V. MODEL PERFORMANCE ----- 47

VI. CONCLUSION ----- 77

LIST OF REFERENCES ----- 78

INITIAL DISTRIBUTION LIST ----- 80





# LIST OF FIGURES

1.	Sigma coordinate system -----	17
2.	Vertical index -----	21
3.	Placement of dependent variables, u, v and h -----	23
4.	Horizontal grid with polar modification -----	25
5.	Flow diagram for a 5-day forecast -----	28
6.	$\pi$ -centered notation and u-centered notation -----	31
7.	Rectangular grid used to represent the globe -----	39
8.	Polar modification of the continuity equation -----	40
9.	Polar modification of the u equation of motion ----	41
10.	Polar modification of the v equation of motion ----	43
11.	Phase angle vs latitude for 16-point N-S grid, wave number 4, phase speed $10^\circ/\text{day}$ and $A=7.0 \times 10^7$ --	51
12.	Phase angle vs latitude for 16-point N-S grid, wave number 8, phase speed $10^\circ/\text{day}$ and $A=1.6 \times 10^8$ --	52
13.	Phase angle vs latitude for 16-point N-S grid, wave number 12, phase speed $10^\circ/\text{day}$ and $A=7.0 \times 10^7$ --	53
14.	Terrain pressure amplitude vs time (hrs) for gravity wave oscillations, wave number 4, $B=0$ , u and v components of the wind=0, Coriolis=0 and $A=7.0 \times 10^7$ -----	54
15.	Percentage of actual advection/theoretical advection vs latitude for wave number 4, Coriolis=0, pressure gradient=0, vertical advection=0, phase speed $10^\circ/\text{day}$ and $A=7.0 \times 10^7$ -----	55
16.	Phase angle vs latitude for 46-point N-S grid, wave number 4, phase speed $-24^\circ/\text{day}$ , $B=0$ and $A=7.0 \times 10^7$ -----	56
17.	Phase angle vs latitude for 46-point N-S grid, wave number 8, phase speed $-8^\circ/\text{day}$ , $B=0$ and $A=1.6 \times 10^8$ -----	59



18.	Phase angle vs latitude for 46-point N-S grid, wave number 12, phase speed $-4^{\circ}/\text{day}$ , $B=0$ and $A=7.0 \times 10^7$ -----	62
19.	Phase angle vs latitude for 46-point N-S grid, wave number 4, phase speed $10^{\circ}/\text{day}$ and $A=7.0 \times 10^7$ --	65
20.	Terrain pressure amplitude vs latitude for initial field and 48-hour forecast, wave number 4, phase speed $10^{\circ}/\text{day}$ and $A=7.0 \times 10^7$ -----	66
21.	Phase angle vs latitude for the 46-point N-S grid, wave number 8, phase speed $10^{\circ}/\text{day}$ and $A=1.6 \times 10^8$ --	69
22.	Terrain pressure amplitude vs latitude for initial field and 48-hour forecast, wave number 8, phase speed $10^{\circ}/\text{day}$ and $A=1.6 \times 10^8$ -----	70
23.	Phase angle vs latitude for 46-point N-S grid, wave number 12, phase speed $10^{\circ}/\text{day}$ and $A=7.0 \times 10^7$ -	73
24.	Terrain pressure amplitude vs latitude for initial field and 48-hour forecast, wave number 12, phase speed $10^{\circ}/\text{day}$ and $A=7.0 \times 10^7$ -----	74



# LIST OF CHARTS

A.	Initial surface pressure analysis for 46-point N-S grid, wave number 4, phase speed $-24^{\circ}/\text{day}$ , $B=0$ and $A = 7.0 \times 10^7$ -----	57
B.	48-hour surface pressure forecast for 46-point N-S grid, wave number 4, phase speed $-24^{\circ}/\text{day}$ , $B=0$ and $A = 7.0 \times 10^7$ -----	58
C.	Initial surface pressure analysis for 46-point N-S grid, wave number 8, phase speed $-8^{\circ}/\text{day}$ , $B=0$ and $A = 1.6 \times 10^8$ -----	60
D.	48-hour surface pressure forecast for 46-point N-S grid, wave number 8, phase speed $-8^{\circ}/\text{day}$ , $B=0$ and $A = 1.6 \times 10^8$ -----	61
E.	Initial surface pressure analysis for 46-point N-S grid, wave number 12, phase speed $-4^{\circ}/\text{day}$ , $B=0$ and $A = 7.0 \times 10^7$ -----	63
F.	48-hour surface pressure forecast for 46-point N-S grid, wave number 12, phase speed $-4^{\circ}/\text{day}$ , $B=0$ and $A = 7.0 \times 10^7$ -----	64
G.	Initial surface pressure analysis for 46-point N-S grid, wave number 4, phase speed $10^{\circ}/\text{day}$ and $A = 7.0 \times 10^7$ -----	67
H.	48-hour surface pressure forecast for 46-point N-S grid, wave number 4, phase speed $10^{\circ}/\text{day}$ and $A = 7.0 \times 10^7$ -----	68
I.	Initial surface pressure analysis for 46-point N-S grid, wave number 8, phase speed $10^{\circ}/\text{day}$ and $A = 1.6 \times 10^8$ -----	71
J.	48-hour surface pressure forecast for 46-point N-S grid, wave number 8, phase speed $10^{\circ}/\text{day}$ and $A = 1.6 \times 10^8$ -----	72
K.	Initial surface pressure analysis for 46-point N-S grid, wave number 12, phase speed $10^{\circ}/\text{day}$ and $A = 7.0 \times 10^7$ -----	75
L.	48-hour surface pressure forecast for 46-point N-S grid, wave number 12, phase speed $10^{\circ}/\text{day}$ and $A = 7.0 \times 10^7$ -----	76



## LIST OF SYMBOLS AND ABBREVIATIONS

A	Arbitrary constant in the stream function
a	Earth's radius
B	Arbitrary constant in the stream function
CDC	Control Data Corporation
$C_p$	Specific heat for dry air at constant pressure
C	Zonal phase speed
$C_0$	Phase speed of the fastest gravity wave
D	Grid distance at the equator
d	Grid distance
E-W	East-West
FNWC	Fleet Numerical Weather Central
F	Zonal flux term
$F_\xi$	Frictional stress (zonal)
$F_\eta$	Frictional stress (meridional)
$F$	Flux term
f	Coriolis parameter
$\bar{f}$	Coriolis parameter at 45° north
$g^u$	Flux term in $\xi$ -equation of motion
$g^v$	Flux term in $\eta$ -equation of motion
G	Meridional flux term
g	Acceleration of gravity
H	Mean depth of a fluid
h	Depth of a fluid
i	Grid index in the $\xi$ -direction
j	Grid index in the $\eta$ -direction





$k$	Vertical grid index
$k_\ell$	Zonal wave length
$m$	$1/(a \cos \phi)$
$m_k$	Zonal wave number
mb	Millibars
NACA	National Advisory Committee on Aeronautics
NPS	Naval Postgraduate School
$N$	Wave number plus one - $m_k+1$
N-S	North-South
$n$	$1/a$
$P$	Pole on the $ij$ index system
$p$	Pressure
$p_0$	1000 mb
$Q$	Moisture source or sink term
$R$	Specific gas constant for dry air
$S$	Stability coefficient
$\dot{S}$	Area-pressure weighted vertical velocity
$t$	Time
$T$	Temperature
$T_p$	Period
$u$	Zonal wind
$\bar{u}$	Mean zonal wind
$\vec{V}$	Horizontal vector velocity
$v$	Meridional wind
$\Delta t$	Time increment
$\alpha$	Specific volume
$\beta$	Derivative of Coriolis with respect to the meridional coordinate



$\eta$	Meridional coordinate of the curvilinear coordinate system
$\Delta\eta$	Distance increment in the meridional direction
$\theta$	Potential temperature
$\kappa$	Specific gas constant/specific heat ( $R/C_p$ )
$\lambda$	Longitude
$\lambda_R$	Radius of deformation ( $\sqrt{gH/\bar{f}}$ )
$\nu$	Angular wave velocity
$\xi$	Zonal coordinate of the curvilinear coordinate system
$\Delta\xi$	Distance increment in zonal direction
$\pi$	Terrain pressure
$\Pi$	Area-weighted terrain pressure
$\sigma$	Dimensionless vertical coordinate
$\Delta\sigma$	Vertical increment in the sigma coordinate system
$\dot{\sigma}$	Measure of vertical velocity
$\phi$	Latitude
$\Phi$	Geopotential
$\psi$	Stream function
$\Omega$	Angular velocity of the earth
$\nabla$	Del operator



## ACKNOWLEDGEMENT

The author wishes to express his thanks to Dr. R. T. Williams for suggesting the project covered in this thesis and for his many hours of patient guidance. Also the author thanks Dr. G. J. Haltiner for his text and course on Numerical Weather Prediction and for reviewing this thesis in preparation for the final draft. Much appreciation is extended to the staff of the W. R. Church Computer Center at the NPS for their excellent support and friendly cooperation. Finally a loving thanks to my wife for enduring over the past year.



## I. INTRODUCTION

Recent research at the NPS in atmospheric global prediction has been primarily concerned with the five-level global primitive equation model initially designed and programmed by Dr. F.J. Winninghoff and further developed by Elias (1973), Mihok (1974), McCollough (1974) and Maher (1974). Their numerical experiments proved valuable but pointed out the inflexibility of the model for research purposes.

Arakawa and Mintz (1974) described an atmospheric global prediction model with a new finite difference formulation and greater vertical resolution. The model employs a new horizontal distribution of variables to improve the geostrophic adjustment process. The purpose of this research was to program and check out a modified version of the new Arakawa scheme. The fundamental approach was to develop a flexible program for use in a number of projects including modeling of tropical circulation. Eventually the model's performance can be compared with the performance of FNWC's global model.

The model was initially developed with two levels and a variable grid to aid in debugging. The atmosphere was treated as adiabatic and frictionless and the water vapor continuity equation was not considered. The initial conditions for all experiments were analytically derived in the same manner as Maher (1974). The advantages of analytic





initial conditions were significant in reducing computer time during check out of the model.



## II. MODEL DESCRIPTION

The differential equations are essentially the same as those described by Arakawa (1972). The integration scheme was carried out on a staggered, spherical, sigma coordinate system. For an adiabatic, frictionless model the primitive equations form a closed set. No sink or source terms were considered in the course of development or check out.

### A. VERTICAL COORDINATE SYSTEM

The model uses the non-dimensional sigma coordinate system as described in Haltiner (1971). The two levels divide the troposphere in half and the tropopause is assumed isobaric. The sigma coordinate is defined as

$$\sigma \equiv \frac{p - p_t}{\pi} , \quad (2.1)$$

where  $p$  is the pressure,  $p_t$  the constant tropopause pressure and  $\pi$  is the terrain pressure. The terrain pressure is further defined as

$$\pi \equiv p_s - p_t , \quad (2.2)$$

where  $p_s$  is the surface pressure. It follows from equation (2.1) that

$$\begin{aligned} \sigma &= 0 \text{ at } p = p_t , \\ \sigma &= 1 \text{ at } p = p_s , \end{aligned} \quad (2.3)$$

which are the vertical boundaries of the coordinate system.



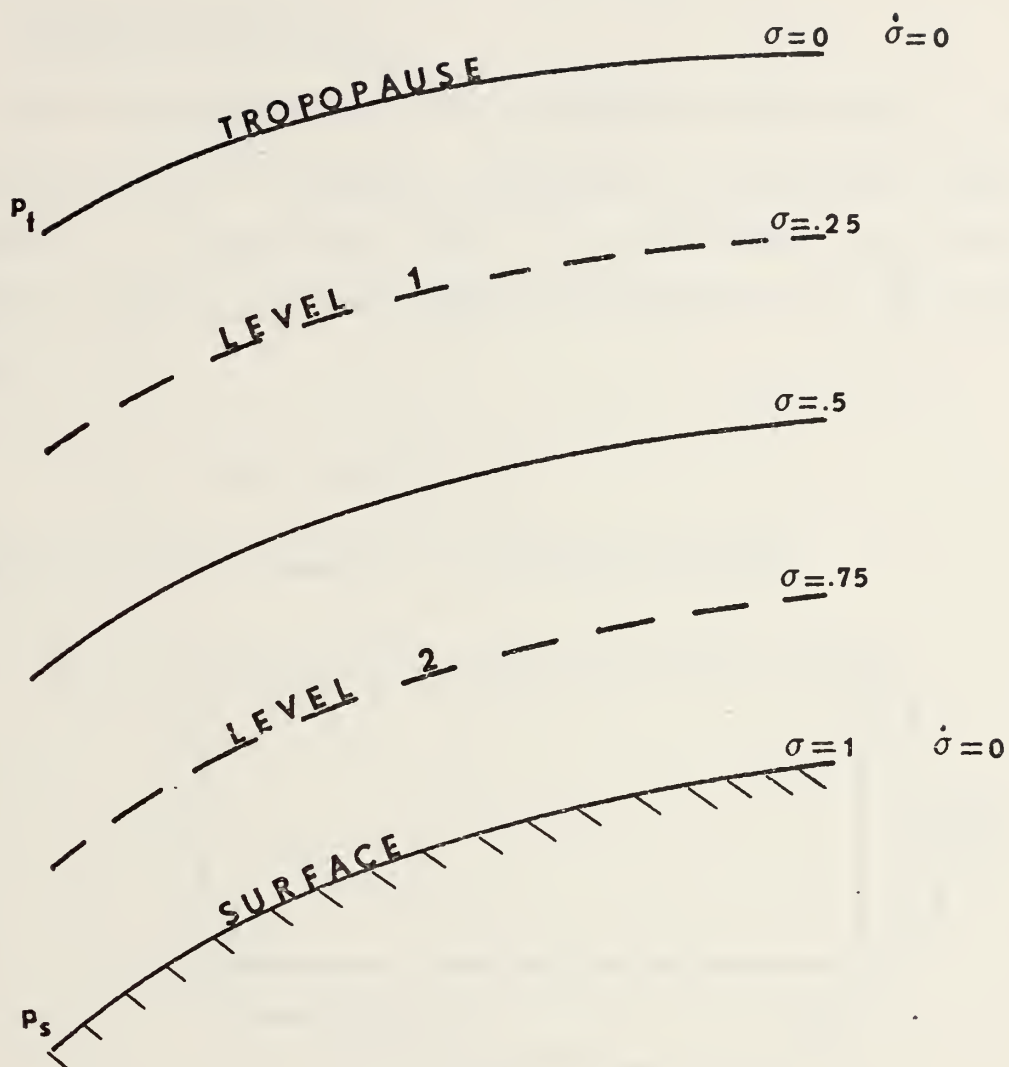


Figure 1. The sigma ( $\sigma$ ) coordinate system as used in the model.  $p_t$  is 200 mb.



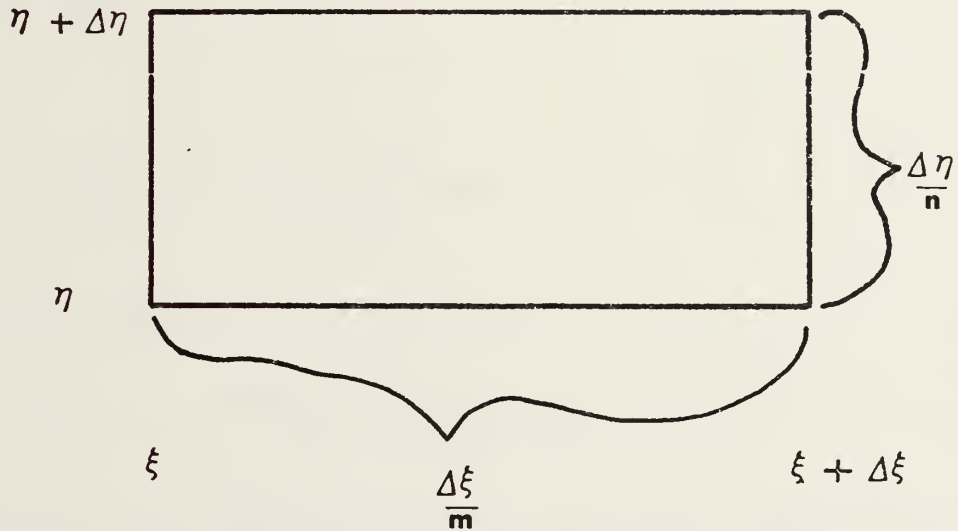
The boundary condition at  $\sigma=1$  is  $\dot{\sigma}=0$  and at  $\sigma=0$  it is assumed that  $\dot{\sigma}=0$  where  $\dot{\sigma}$  is defined as  $d\sigma/dt$ .

## B. PRIMITIVE EQUATIONS

The continuous form of the primitive equations is described in the orthogonal curvilinear coordinates  $\xi$  and  $\eta$  where  $\xi = \lambda$  (longitude) and  $\eta = \phi$  (latitude). An area element is  $\frac{1}{mn}\Delta\xi\Delta\eta$  and the lengths of the sides are  $\frac{\Delta\xi}{m}$  and  $\frac{\Delta\eta}{n}$ , where

$$\frac{1}{m} = a \cos \phi \text{ and } \frac{1}{n} = a.$$

The difference element is illustrated below.



The mass continuity equation is

$$\frac{\partial}{\partial t}\left(\frac{\pi}{mn}\right) + \frac{\partial}{\partial \xi}\left(\pi \frac{u}{n}\right) + \frac{\partial}{\partial \eta}\left(\pi \frac{v}{m}\right) + \frac{\partial}{\partial \sigma}\left(\frac{\pi \dot{\sigma}}{mn}\right) = 0. \quad (2.4)$$





The  $\xi$ -component of the horizontal equation of motion is

$$\begin{aligned} & \frac{\partial}{\partial t}(\frac{\pi}{mn}u) + \frac{\partial}{\partial \xi}(\frac{\pi u}{n}u) + \frac{\partial}{\partial \eta}(\frac{\pi v}{m}u) + \frac{\partial}{\partial \sigma}(\frac{\pi \dot{\sigma}}{mn}u) \\ & - [\frac{f}{mn} + (v\frac{\partial}{\partial \xi}\frac{1}{n} - u\frac{\partial}{\partial \eta}\frac{1}{m})]\pi v + \frac{\pi}{n}[\frac{\partial \Phi}{\partial \xi} + \sigma\alpha\frac{\partial \pi}{\partial \xi}] = \frac{\pi}{mn}F_{\xi} . \end{aligned} \quad (2.5)$$

The  $\eta$ -component of the horizontal equation of motion is

$$\begin{aligned} & \frac{\partial}{\partial t}(\frac{\pi}{mn}v) + \frac{\partial}{\partial \xi}(\frac{\pi u}{n}v) + \frac{\partial}{\partial \eta}(\frac{\pi v}{m}v) + \frac{\partial}{\partial \sigma}(\frac{\pi \dot{\sigma}}{mn}v) \\ & + [\frac{f}{mn} + (v\frac{\partial}{\partial \xi}\frac{1}{n} - u\frac{\partial}{\partial \eta}\frac{1}{m})]\pi u + \frac{\pi}{m}[\frac{\partial \Phi}{\partial \eta} + \sigma\alpha\frac{\partial \pi}{\partial \eta}] = \frac{\pi}{mn}F_{\eta} . \end{aligned} \quad (2.6)$$

The first law of thermodynamics is written in the following manner:

$$C_p \frac{dT}{dt} = \omega\alpha + Q, \quad (2.7)$$

where

$$\omega = \frac{dp}{dt} = \pi\dot{\sigma} + \sigma(\frac{\partial}{\partial t} + \vec{V} \cdot \nabla)\pi \quad (2.8)$$

and the flux form is

$$\frac{\partial}{\partial t}(\pi C_p T) + \nabla_{\sigma} \cdot (\pi \vec{V} C_p T) + \frac{\partial}{\partial \sigma}(\pi \dot{\sigma} C_p T) = \pi(\omega\alpha + Q). \quad (2.9)$$

Using the relationship for potential temperature,

$$T = \theta(\frac{p}{p_0})^{\kappa}, \quad (2.10)$$

the final form in curvilinear coordinates is



$$\begin{aligned}
& \frac{\partial}{\partial t} \left( \frac{\pi}{mn} C_p T \right) + \frac{\partial}{\partial \xi} \left( \frac{\pi u}{n} C_p T \right) + \frac{\partial}{\partial \eta} \left( \frac{\pi v}{m} C_p T \right) + \left( \frac{p}{p_0} \right)^{\kappa} \frac{\partial}{\partial \sigma} \left( \frac{\pi \dot{\sigma}}{mn} C_p \theta \right) \\
& = \pi \sigma \alpha \left[ \frac{\partial}{\partial t} \left( \frac{\pi}{mn} \right) + \frac{u}{n} \frac{\partial \pi}{\partial \xi} + \frac{v}{m} \frac{\partial \pi}{\partial \eta} \right] + \frac{\pi}{mn} Q .
\end{aligned} \tag{2.11}$$

The equation of state is

$$\alpha = \frac{RT}{p} \tag{2.12}$$

and the hydrostatic relationship is

$$\delta \Phi = -\pi \alpha \delta \sigma . \tag{2.13}$$

A complete set of symbols for the above equation may be found in the front of this report.

### C. VERTICAL INDEX

The index  $k$  is used to identify the vertical levels. At the upper boundary  $k=0$ ,  $p=p_t$  and at the lower boundary  $k=K+1$  and  $p=p_s$ . The variables  $\vec{V}$  and  $T$  are carried at the odd levels while  $\pi \dot{\sigma}$  is carried at the even levels. The following definitions are required to complete the vertical system:

$$\Delta \sigma_k \equiv \sigma_{k+1} - \sigma_{k-1} , \tag{2.14}$$

$$\sum_{k=1}^{K'} \Delta \sigma_k \equiv 1 , \tag{2.15}$$

where the summation is over odd  $k$  (see figure 2).



INDEX $k$	COMPUTED VARIABLES	SIGMA
<u>0</u>	$\pi \dot{\sigma} \equiv 0$	$\sigma = 0$
<u>1</u>	$\nabla T \underline{\Phi}$	
<u>2</u>	$\pi \dot{\sigma}$	$\sigma = \sigma_2$
<u>3</u>	$\nabla T \underline{\Phi}$	
<u><math>k-2</math></u>	$\nabla T \underline{\Phi}$	
<u><math>k-1</math></u>	$\pi \dot{\sigma}$	$\sigma = \sigma_{k-1}$
<u><math>k</math></u>	$\nabla T \underline{\Phi}$	
<u><math>k+1</math></u>	$\pi \dot{\sigma}$	$\sigma = \sigma_{k+1}$
<u><math>k+2</math></u>	$\nabla T \underline{\Phi}$	
<u><math>K-2</math></u>	$\nabla T \underline{\Phi}$	
<u><math>K-1</math></u>	$\pi \dot{\sigma}$	$\sigma = \sigma_{K-1}$
<u><math>K</math></u>	$\nabla T \underline{\Phi}$	
<u><math>K+1</math></u>	$\pi \dot{\sigma} \equiv 0$	$\sigma = 1$

### V E R T I C A L I N D E X

Figure 2. In the above figure  $k$  is a variable vertical index, sigma ( $\sigma$ ) is the dimensionless vertical coordinate,  $\vec{V}$  is the horizontal vector velocity,  $\pi$  is the terrain pressure,  $\dot{\sigma}$  is the vertical velocity,  $T$  is the temperature and  $\Phi$  is the geopotential.



#### D. HORIZONTAL GRID AND DISTRIBUTION OF VARIABLES

The selection of the horizontal distribution of variables is a function of two distinct processes. The first is proper simulation of the geostrophic adjustment process and the second is proper simulation of slowly changing quasi-geostrophic motion after it has been established by geostrophic adjustment. As shown by Winninghoff (1968) geostrophic adjustment depends on how the variables are distributed over the grid points. Winninghoff used the following equations, which are the simplest ones in which geostrophic adjustment can take place, to demonstrate five possibilities for the placement of the dependent variables:

$$\frac{du}{dt} - \bar{f}v + g\frac{\partial h}{\partial x} = 0 , \quad (2.16)$$

$$\frac{dv}{dt} + \bar{f}u + g\frac{\partial h}{\partial y} = 0 , \quad (2.17)$$

$$\frac{dh}{dt} + h\left(\frac{\partial u}{\partial x} + \frac{\partial v}{\partial y}\right) = 0 . \quad (2.18)$$

The above equations represent an incompressible, homogenous, non-viscous, hydrostatic, rotational fluid with a flat bottom and a free surface, where  $u$  and  $v$  are the velocity components,  $h$  is the depth of the fluid,  $\bar{f}$  is a constant Coriolis parameter,  $t$  is the time,  $x$  and  $y$  are the horizontal coordinates and  $g$  is gravity. The five possible distributions of the dependent variables  $h$ ,  $v$  and  $u$  are shown in figure 3. Scheme B was used in the Mintz-Arakawa two-level global circulation model (Langlois and Kwok, 1969) and





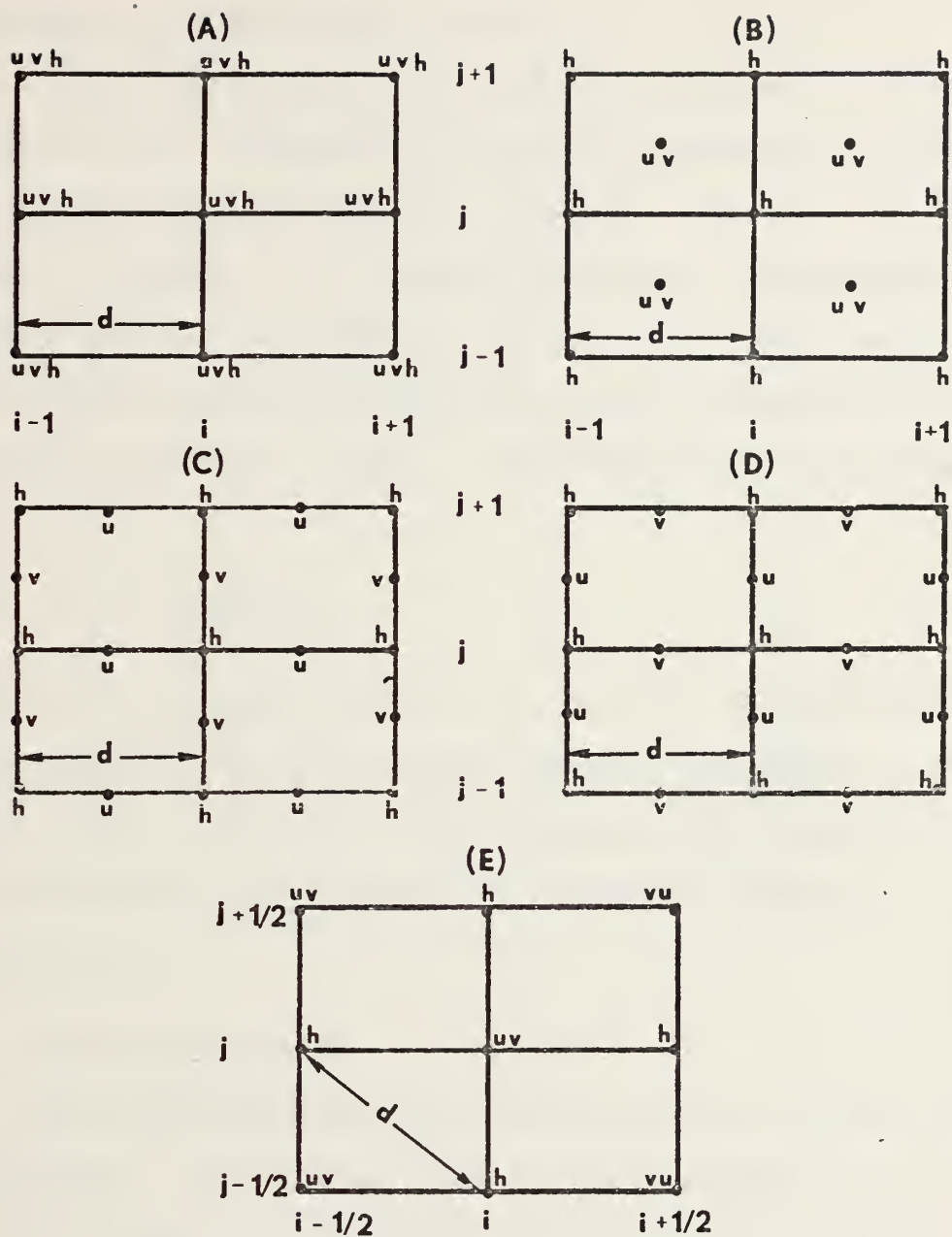


Figure 3. The above figure represents the placement of the dependent variables  $h$ ,  $v$  and  $u$  where  $h$  is the depth of the fluid,  $u$  and  $v$  are the velocity components and  $d$  is the grid distance (for the simplest case of geostrophic adjustment).



scheme E is used in the global model now under further development at FNWC (Maher, 1974).

In the one-dimensional case it was shown that both scheme B and C adequately simulated geostrophic adjustment. In the two-dimensional case, however, scheme C was shown most satisfactory to simulate geostrophic adjustment, except where  $\lambda_R/d$  is less than or close to one. The quantity  $\lambda_R$  is the Rossby radius of deformation and  $d$  is the grid distance (Arakawa and Mintz, 1974). The Rossby radius of deformation is

$$\lambda_R = \sqrt{gH} / \bar{f}$$

where  $H$  is the mean value of  $h$ ,  $g$  is the acceleration of gravity and  $\bar{f}$  is the constant Coriolis parameter. The condition  $\lambda_R/d \leq 1$  is an abnormal case, therefore, the horizontal distribution of variables is based on scheme C. (See figure 4.)

#### E. TIME DIFFERENCING

The time differencing is carried out in thirty minute sequences. The initial step in each sequence is a two part Matsuno scheme represented by the following notation:

$$F^* = F^t + \Delta t \frac{\partial F^t}{\partial t} \quad (\text{Forward}), \quad (2.19)$$

$$F^{t+1} = F^t + \Delta t \frac{\partial F^*}{\partial t} \quad (\text{Backward}) . \quad (2.20)$$



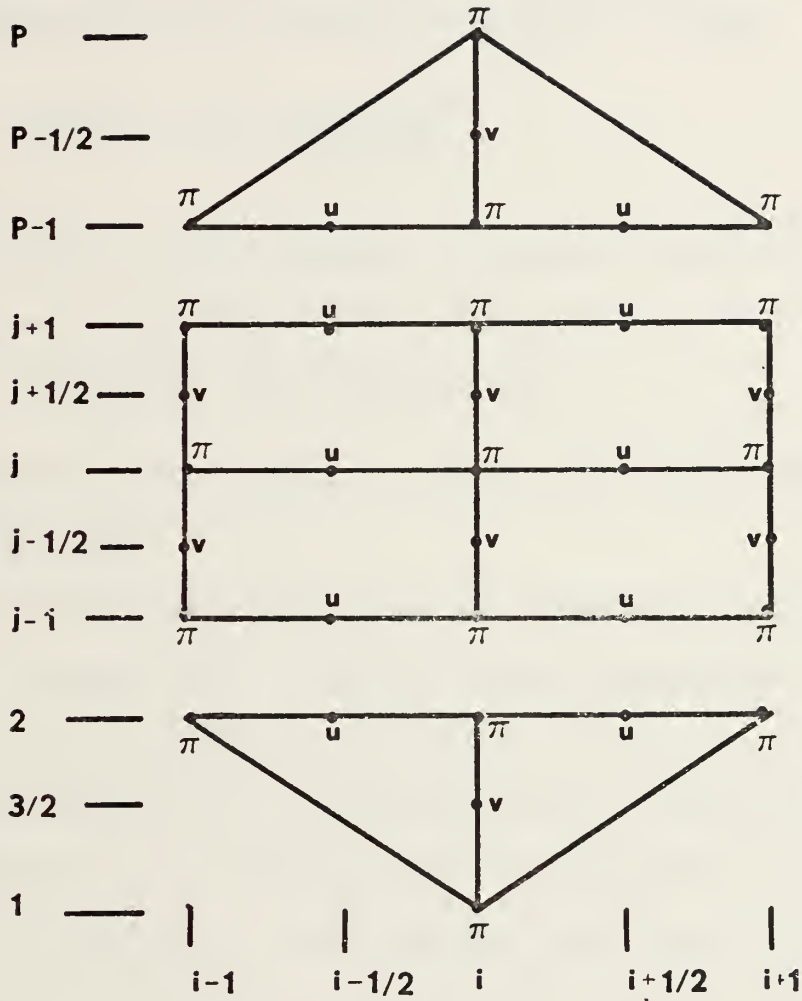


Figure 4. The above figure represents the horizontal distribution of dependent variables with polar modification.  $P$  in the  $ij$  index system represents the north pole,  $1$  represents the south pole and  $i$  represents a meridian.  $\pi$  represents the variables  $T$ ,  $\Phi$  and  $\pi$  carried at " $\pi$ -points."  $u$  and  $v$  are the horizontal components of velocity.



F is a vector representing the dependent variables. The superscript t represents the time step, the superscript \* represents the results of an intermediate step and  $\Delta t$  is the time interval of a single step. The remaining time steps in a sequence use the leapfrog scheme as follows:

$$F^{t+1} = F^{t-1} + 2\Delta t \frac{\partial F^t}{\partial t} . \quad (2.21)$$

At the end of each sequence provision is made for the calculation of the source terms. The present model doesn't incorporate source term calculations.

#### F. AVERGING THE PRESSURE GRADIENT AND ZONAL MASS FLUX NEAR THE POLES

A problem that may arise at higher latitudes is computational instability. Computational instability is a result of the convergence of the meridians to the poles causing greatly reduced grid distances along a latitude circle. Therefore, some technique must be employed to eliminate the stability problem. One technique involves reducing  $\Delta t$  in higher latitudes but it would impose serious programming difficulties and require more computer time. Another technique would be to reduce the number of grid points in a latitude circle at higher latitudes, however, it also would impose programming difficulties. A third technique is zonal smoothing which was developed by Arakawa and Mintz (1974). Smoothing preserves the integrity of the horizontal grid while maintaining a constant time step. Zonal smoothing is





used in this model and also by FNWC to eliminate computational instability at high latitudes.

Zonal smoothing involves expanding the pressure gradient and zonal mass flux into a Fourier series and reducing the amplitude of each wave component by a factor

$$S = \frac{D \cos \phi}{C_0 \Delta t \sin (m_k d)} \quad (2.22)$$

where

$S$  = Stability Coefficient,

$D$  = Grid distance at the equator,

$C_0$  = Phase speed of the fastest gravity wave,

$\Delta t$  = Time step,

$m_k$  = Wave number,

$d$  = Grid distance in degrees.

If the value of  $S$  is greater than one, smoothing is not required (Arakawa and Mintz, 1974). As pointed out by Arakawa the smoothing operation does not smooth the fields of variables, because it is simply a generation of multiple point difference quotients. The bar operators in Chapter III indicate zonal smoothing.

#### G. PROGRAM FORMAT

The program format was patterned after the Mintz-Arakawa two-level global model as described by Gates, et al. (1971) and Langlois and Kwok (1969) and modified to include scheme C distribution of variables and a Matsuno-leapfrog time integration scheme. Figure 5 gives a simplified flow diagram



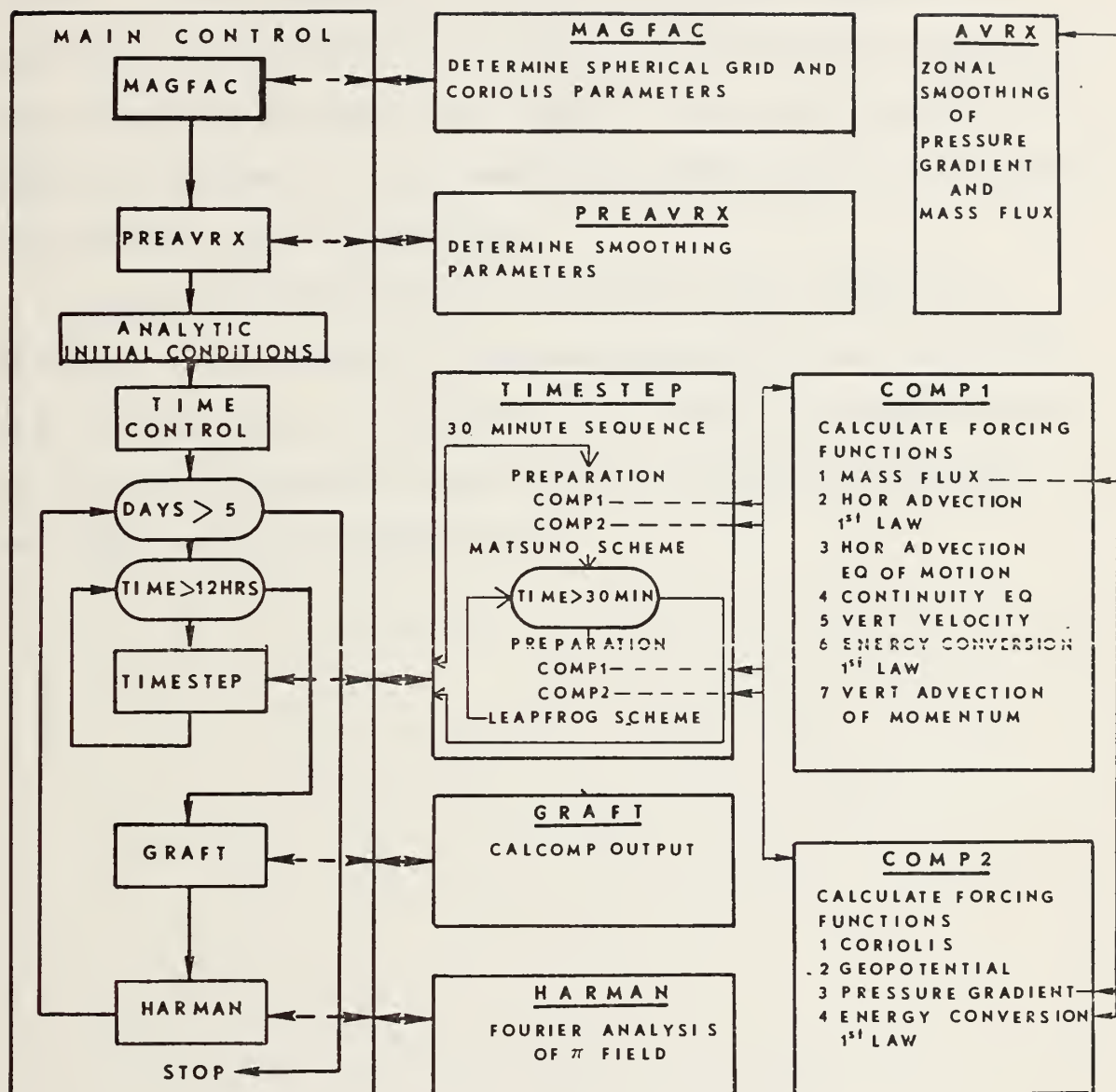


Figure 5. A simplified flow diagram for 5-day forecast using analytic initial conditions.



for a five-day forecast. The main program controls the overall time period of the forecast as well as input and output. Time integration for each 30-minute sequence is controlled by subroutine Timestep. The forcing functions are calculated in Comp 1 and Comp 2 with zonal smoothing applied as necessary. The remaining subroutines are peripheral to the main flow of the model.

A main consideration in the program was flexibility, therefore, the vertical structure along with the horizontal grid are variable. The model can be used to simulate several different horizontal and vertical structures including the FNWC's 5-level global model.



### III. FINITE DIFFERENCE EQUATION

The finite difference equations given in this chapter were developed by Arakawa and Mintz (1974). The advection terms of the equation of motion were modified to eliminate the diagonal flux calculations. The short-term performance should not be affected by elimination of the diagonal flux terms and considerable computer time was saved.

The notation used in this chapter represents the specific variable centered in the  $ij$  index system. Figure 6 contains an example of " $\pi$ -centered" and "u-centered" notation.  $\pi$ -centered notation is used for the continuity equation and the thermodynamic equation in which the dependent variable is carried at a  $\pi$ -point. U-centered notation is used for the  $\xi$ -component of the equation of motion and v-centered notation is used for the  $\eta$ -component of the equation of motion. Refer to the front of the report for a complete list of symbols.

#### A. CONTINUITY EQUATION

The following form is used for the continuity equation given in equation (2.4):

$$\begin{aligned} \frac{\partial \Pi_{i,j}}{\partial t} + F_{i+\frac{1}{2},j}^k - F_{i-\frac{1}{2},j}^k + G_{i,j+\frac{1}{2}}^k - G_{i,j-\frac{1}{2}}^k \\ + \frac{1}{\Delta \sigma^k} (\dot{S}_{i,j}^{k+1} - \dot{S}_{i,j}^{k-1}) = 0 , \end{aligned} \quad (3.1)$$





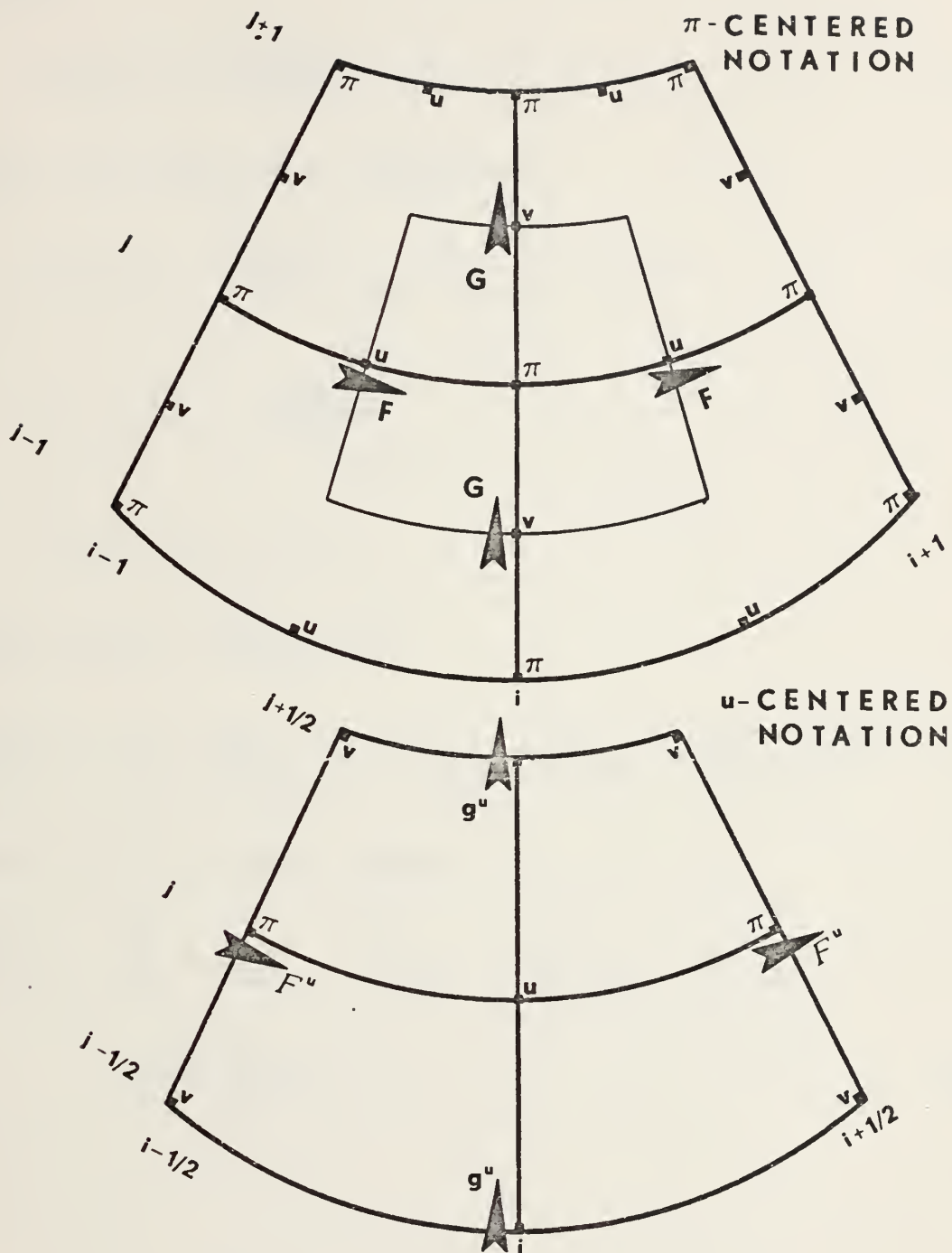


Figure 6. An example of the notation used to describe the finite difference equations. The continuity equation is described on a "π-centered" grid in which the  $F$  and  $G$  symbols are flux calculations in their respective directions. The "u-centered" grid is an example used to describe the  $\xi$ -component of the equation of motion where  $F^u$  and  $g^u$  are also flux calculations.



where

$$\overline{F_{i+\frac{1}{2},j}^k} = \frac{1}{2} \left( u \frac{\Delta \eta}{n} \right)_{i+\frac{1}{2},j}^k (\pi_{i+1,j} + \pi_{i,j}) , \quad (3.2)$$

(bar indicates zonal smoothing)

$$G_{i,j+\frac{1}{2}}^k = \frac{1}{2} \left( v \frac{\Delta \xi}{m} \right)_{i,j+\frac{1}{2}}^k (\pi_{i,j+1} + \pi_{i,j}) , \quad (3.3)$$

$$\Pi_{i,j} \equiv \pi_{i,j} \left( \frac{\Delta \xi \Delta \eta}{mn} \right)_{i,j} ,$$

$$\dot{S}_{i,j} \equiv \Pi_{i,j} \dot{\sigma}_{i,j} .$$

The tendency equation is

$$\frac{\partial \Pi_{i,j}}{\partial t} = - \sum_{k=1}^{K'} (F_{i+\frac{1}{2},j}^k - F_{i-\frac{1}{2},j}^k + G_{i,j+\frac{1}{2}}^k - G_{i,j-\frac{1}{2}}^k) \Delta \sigma^k . \quad (3.4)$$

The vertical motion equation is

$$\begin{aligned} \dot{S}_{i,j}^{k+1} = & - \sum_{k=1}^{K'} (F_{i+\frac{1}{2},j}^k - F_{i-\frac{1}{2},j}^k + G_{i,j+\frac{1}{2}}^k - G_{i,j-\frac{1}{2}}^k) \Delta \sigma^k \\ & - \sigma^{k+1} \frac{\partial \Pi_{i,j}}{\partial t} . \end{aligned} \quad (3.5)$$



## B. PRESSURE GRADIENT TERM AND HYDROSTATIC EQUATION

### 1. Hydrostatic Equation

The geopotential for a level K is given by

$$\begin{aligned} \phi_{i,j}^K = & \phi_{i,j}^S + \sum_{k=1}^K \pi_{i,j} \sigma^k \frac{RT_{i,j}^k}{p_{i,j}^k} \Delta \sigma^k \\ & - \sum_{k=1}^{K-2} \sigma^{k+1} C_p \hat{\theta}_{i,j}^{k+1} \left[ \left( \frac{p^{k+2}}{p_0} \right)_{i,j}^\kappa - \left( \frac{p^k}{p_0} \right)_{i,j}^\kappa \right], \end{aligned} \quad (3.6)$$

where  $\phi^S$  is the geopotential at the surface,

$$\hat{\theta}^{k+1} \equiv \frac{\ln \theta^k - \ln \theta^{k+2}}{\frac{1}{\theta^{k+2}} - \frac{1}{\theta^k}}.$$

Given  $\phi^K$ , the geopotential for the remaining levels is found using the following relationship:

$$\phi_{i,j}^k - \phi_{i,j}^{k+2} = C_p \left[ \left( \frac{p^{k+2}}{p_0} \right)_{i,j}^\kappa - \left( \frac{p^k}{p_0} \right)_{i,j}^\kappa \right] \hat{\theta}_{i,j}^{k+1}. \quad (3.7)$$

### 2. $\eta$ -component of the Pressure Gradient Force

The pressure gradient force in the meridional equation of motion as given in equation (2.6) is

$$\begin{aligned} & - \frac{\Delta \xi}{m_j} \frac{1}{2} [(\pi_{i,j+\frac{1}{2}} + \pi_{i,j-\frac{1}{2}})(\phi_{i,j+\frac{1}{2}}^k - \phi_{i,j-\frac{1}{2}}^k) \\ & + ((\pi \sigma \alpha)_{i,j+\frac{1}{2}}^k + (\pi \sigma \alpha)_{i,j-\frac{1}{2}}^k)(\pi_{i,j+\frac{1}{2}} - \pi_{i,j-\frac{1}{2}})] , \end{aligned} \quad (3.8)$$



where

$$(\pi\sigma\alpha)_{i,j+\frac{1}{2}}^k = \pi_{i,j+\frac{1}{2}} \sigma^k \frac{RT_{i,j+\frac{1}{2}}^k}{p_{i,j+\frac{1}{2}}} .$$

### 3. $\xi$ -component of the Pressure Gradient Force

The pressure gradient force in the zonal equation of motion as given in equation (2.5) is

$$\begin{aligned} & - \frac{\Delta\eta}{n_j} \frac{\frac{1}{2}[(\pi_{i+1,j} + \pi_{i,j})(\phi_{i+1,j}^k - \phi_{i,j}^k)]}{+ ((\pi\sigma\alpha)_{i+1,j}^k + (\pi\sigma\alpha)_{i,j}^k)(\pi_{i+1,j} - \pi_{i,j})] } . \end{aligned} \quad (3.9)$$

### C. MOMENTUM FLUXES

The zonal momentum flux as given in equation (2.5) is

$$\begin{aligned} & \frac{\partial}{\partial t}(\Pi_{i,j}^u u_{i,j}^k) + \frac{1}{2}[F_{i+\frac{1}{2},j}^u(u_{i+1,j} + u_{i,j})^k \\ & - F_{i-\frac{1}{2},j}^u(u_{i,j} + u_{i-1,j})^k + g_{i,j+\frac{1}{2}}^u(u_{i,j+1} + u_{i,j})^k \\ & - g_{i,j-\frac{1}{2}}^u(u_{i,j} + u_{i,j-1})^k] + \frac{1}{\Delta\sigma^k} \frac{1}{2}[\dot{S}_{i,j}^{u,k+1}(u_{i,j}^{k+2} + u_{i,j}^k) \\ & - \dot{S}_{i,j}^{u,k-1}(u_{i,j}^k + u_{i,j}^{k-2})] , \end{aligned} \quad (3.10)$$

where

$$\Pi_{i,j}^u \equiv \frac{1}{2}(\Pi_{i+\frac{1}{2},j} + \Pi_{i-\frac{1}{2},j}) ,$$





$$\dot{S}_{i,j}^u \equiv \frac{1}{2}(\dot{S}_{i+\frac{1}{2},j} + \dot{S}_{i-\frac{1}{2},j}) .$$

$F^u$  and  $g^u$  are defined as follows:

$$F_{i+\frac{1}{2},j}^u \equiv \frac{1}{4}(F_{i+\frac{1}{2},j+1}^* + 2F_{i+\frac{1}{2},j}^* + F_{i+\frac{1}{2},j-1}^*) , \quad (3.11)$$

$$g_{i,j+\frac{1}{2}}^u \equiv \frac{1}{4}(G_{i+\frac{1}{2},j}^* + G_{i+\frac{1}{2},j+1}^* + G_{i-\frac{1}{2},j}^* + G_{i-\frac{1}{2},j+1}^*) , \quad (3.12)$$

where

$$F_{i,j}^* \equiv \frac{1}{2}(F_{i+\frac{1}{2},j} + F_{i-\frac{1}{2},j}) , \quad (3.13)$$

$$G_{i,j}^* \equiv \frac{1}{2}(G_{i,j+\frac{1}{2}} + G_{i,j-\frac{1}{2}}) . \quad (3.14)$$

The meridional momentum flux is similar to equation (3.10) with  $u$  replaced by  $v$ .  $F^v$ ,  $g^v$ ,  $\Pi^v$  and  $\dot{S}^v$  take the following form:

$$F_{i+\frac{1}{2},j}^v \equiv \frac{1}{4}(F_{i+1,j+\frac{1}{2}}^* + F_{i,j+\frac{1}{2}}^* + F_{i,j-\frac{1}{2}}^* + F_{i+1,j-\frac{1}{2}}^*) , \quad (3.15)$$

$$g_{i,j+\frac{1}{2}}^v \equiv \frac{1}{4}(G_{i+1,j+\frac{1}{2}}^* + 2G_{i,j+\frac{1}{2}}^* + G_{i-1,j+\frac{1}{2}}^*) , \quad (3.16)$$

$$\Pi_{i,j}^v \equiv \frac{1}{2}(\Pi_{i,j+\frac{1}{2}} + \Pi_{i,j-\frac{1}{2}}) , \quad (3.17)$$

$$\dot{S}_{i,j}^v \equiv \frac{1}{2}(\dot{S}_{i,j+\frac{1}{2}} + \dot{S}_{i,j-\frac{1}{2}}) . \quad (3.18)$$

$F^*$  is defined by equation (3.13) and  $G^*$  by equation (3.14).



#### D. CORIOLIS FORCE

A variable  $C_{i,j}^k$  is defined at  $\pi$ -points by

$$C_{i,j}^k \equiv f_{i,j} \left( \frac{\Delta \xi \Delta \eta}{mn} \right)_j - \frac{1}{2} (u_{i+\frac{1}{2},j} + u_{i-\frac{1}{2},j})^k$$

$$\left[ \left( \frac{\Delta \xi}{m} \right)_{j+\frac{1}{2}} - \left( \frac{\Delta \xi}{m} \right)_{j-\frac{1}{2}} \right],$$

where  $f_{i,j}$  is the Coriolis parameter.

The zonal-component of the Coriolis force as given in equation (2.5) is

$$\frac{1}{4} [\pi_{i+\frac{1}{2},j} C_{i+\frac{1}{2},j}^k (v_{i+\frac{1}{2},j+\frac{1}{2}} + v_{i+\frac{1}{2},j-\frac{1}{2}})^k$$

$$+ \pi_{i-\frac{1}{2},j} C_{i-\frac{1}{2},j}^k (v_{i-\frac{1}{2},j+\frac{1}{2}} + v_{i-\frac{1}{2},j-\frac{1}{2}})^k] . \quad (3.19)$$

The meridional-component as given in equation (2.6) is

$$-\frac{1}{4} [\pi_{i,j-\frac{1}{2}} C_{i,j-\frac{1}{2}}^k (u_{i+\frac{1}{2},j-\frac{1}{2}} + u_{i-\frac{1}{2},j-\frac{1}{2}})^k$$

$$+ \pi_{i,j+\frac{1}{2}} C_{i,j+\frac{1}{2}}^k (u_{i+\frac{1}{2},j+\frac{1}{2}} + u_{i-\frac{1}{2},j+\frac{1}{2}})^k] . \quad (3.20)$$

#### E. THERMODYNAMIC ENERGY EQUATION

The thermodynamic equation corresponding to equation (2.11) may be written as



$$\begin{aligned}
& \frac{\partial}{\partial t} (\Pi_{i,j} T_{i,j}^k) + F_{i+\frac{1}{2},j}^k \left( \frac{T_{i+1,j} + T_{i,j}}{2} \right)^k \\
& - F_{i-\frac{1}{2},j}^k \left( \frac{T_{i,j} + T_{i-1,j}}{2} \right)^k + G_{i,j+\frac{1}{2}}^k \left( \frac{T_{i,j+1} + T_{i,j}}{2} \right)^k \\
& - G_{i,j-\frac{1}{2}}^k \left( \frac{T_{i,j} + T_{i,j-1}}{2} \right)^k + \frac{1}{\Delta \sigma^k} [\dot{S}_{i,j}^{k+1} \left( \frac{p_{i,j}^k}{p_0} \right)^k \hat{\theta}_{i,j}^{k+1} \\
& - \dot{S}_{i,j}^{k-1} \left( \frac{p_{i,j}^{k-1}}{p_0} \right)^k \hat{\theta}_{i,j}^{k-1}] = \frac{1}{C_p} [(\pi \sigma \alpha)_{i,j}^k \frac{\partial \Pi_{i,j}}{\partial t} \\
& + \frac{1}{4} \{ (u \frac{\Delta \eta}{n})_{i+\frac{1}{2},j}^k ((\pi \sigma \alpha)_{i+1,j}^k + (\pi \sigma \alpha)_{i,j}^k) (\pi_{i+1,j} - \pi_{i,j}) \\
& + (u \frac{\Delta \eta}{n})_{i-\frac{1}{2},j}^k ((\pi \sigma \alpha)_{i,j}^k + (\pi \sigma \alpha)_{i-1,j}^k) (\pi_{i,j} - \pi_{i-1,j}) \\
& + (v \frac{\Delta \xi}{m})_{i,j+\frac{1}{2}}^k ((\pi \sigma \alpha)_{i,j+1}^k + (\pi \sigma \alpha)_{i,j}^k) (\pi_{i,j+1} - \pi_{i,j}) \\
& + (v \frac{\Delta \xi}{m})_{i,j-\frac{1}{2}}^k ((\pi \sigma \alpha)_{i,j}^k + (\pi \sigma \alpha)_{i,j-1}^k) (\pi_{i,j} - \pi_{i,j-1}) \} \\
& + \Pi_{i,j} Q_{i,j}^k] . \tag{3.21}
\end{aligned}$$

## F. POLAR MODIFICATION

The poles of a spherical coordinate system are singular points and polar velocity components cannot be defined. Terrain pressure ( $\pi$ ) at the poles can change as a result of meridional flux at all points  $P-\frac{1}{2}$  and  $P+\frac{1}{2}$  where  $v$  is carried.



The continuity equation is modified at the poles by omitting all undefined flux terms. Each pole is treated as a series of points in order to facilitate programming (see figure 7). Each index  $i, P$  represents the shaded area shown in figure 8. The continuity equation is integrated at each point representing the pole and then averaged to determine a polar value. The thermodynamic equation and the vertical velocity are treated in a similar manner. The advective terms in the equation of motion are given special treatment. The remaining terms in the equation of motion are unchanged except in the case where they are undefined and omitted.

### 1. The Advective Terms in the $\xi$ -component of the Equation of Motion

The polar modification of the  $\xi$ -component of the equation of motion is shown in figure 9. It was modified from the Arakawa scheme by eliminating the diagonal flux terms. The following form is used:

$$\begin{aligned}
 & \frac{\partial (\Pi^u u^k)}{\partial t}_{i, P-1} + \frac{1}{2} [ F_{i+\frac{1}{2}, P-1}^{*u} (u_{i, P-1} + u_{i+1, P})^k \\
 & - F_{i-\frac{1}{2}, P-1}^{*u} (u_{i, P-1} + u_{i-1, P-1})^k - g_{i, P-3/2}^u (u_{i, P-1} + u_{i, P-2})^k ] \\
 & + \frac{1}{\Delta \sigma^k} \frac{1}{2} [ \dot{S}^{u, k+1} (u_{i, P-1}^{k+2} + u_{i, P-1}^k) - \dot{S}^{u, k-1} (u_{i, P-1}^k + u_{i, P-1}^{k-2}) ] ,
 \end{aligned}
 \tag{3.22}$$

where

$$F_{i-\frac{1}{2}, P-1}^{*u} \equiv \frac{1}{4} (4F_{i-\frac{1}{2}, P-1}^{*u} + F_{i-\frac{1}{2}, P-2}^{*u}) ,$$





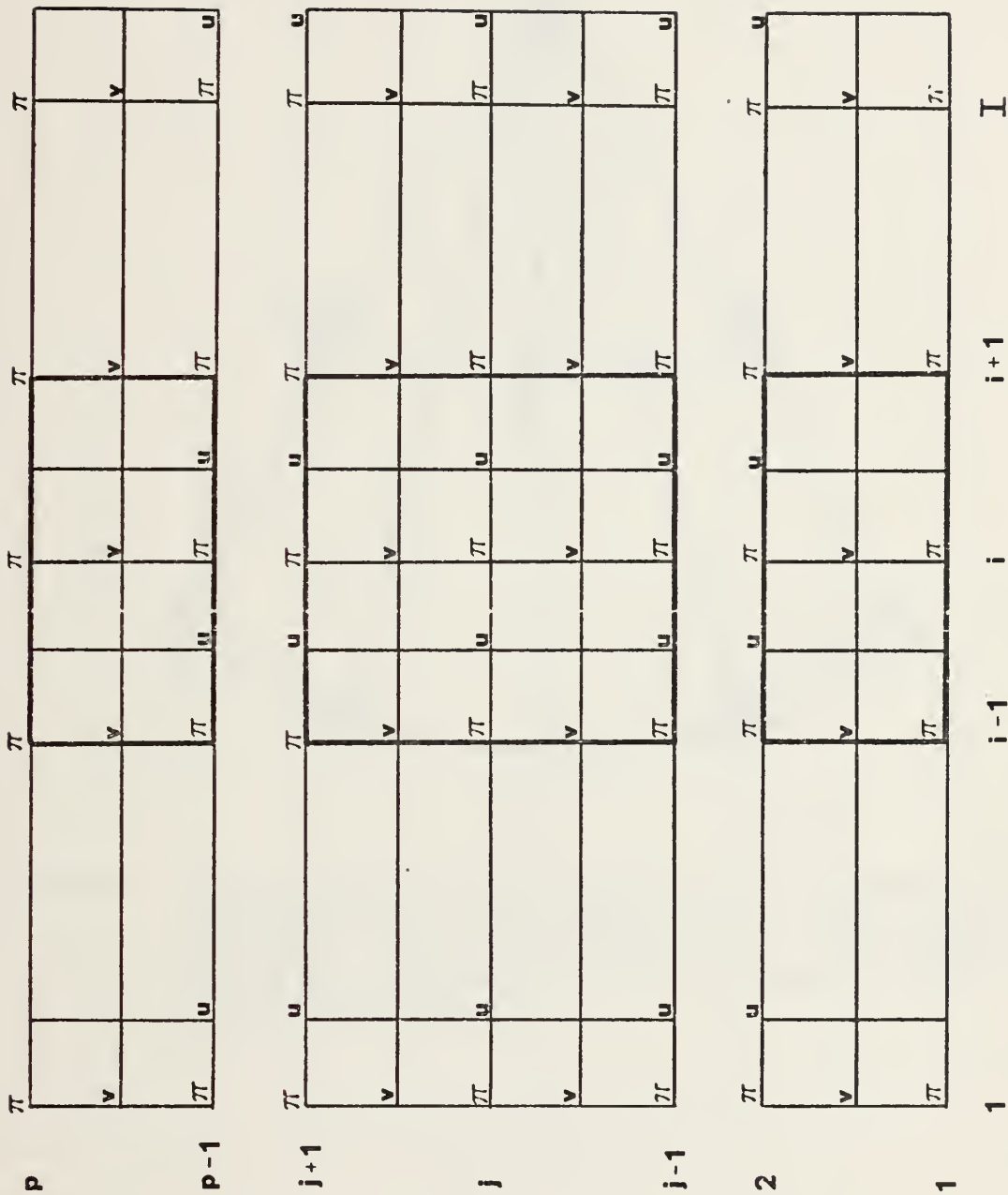


Figure 7. The rectangular grid used to represent the globe treats the poles as a series of points and requires averaging to determine the polar value of  $\pi$ ,  $T$  and  $S$ . The  $u$ , and  $v$  equations of motion are modified at the poles and treated in a separate manner.



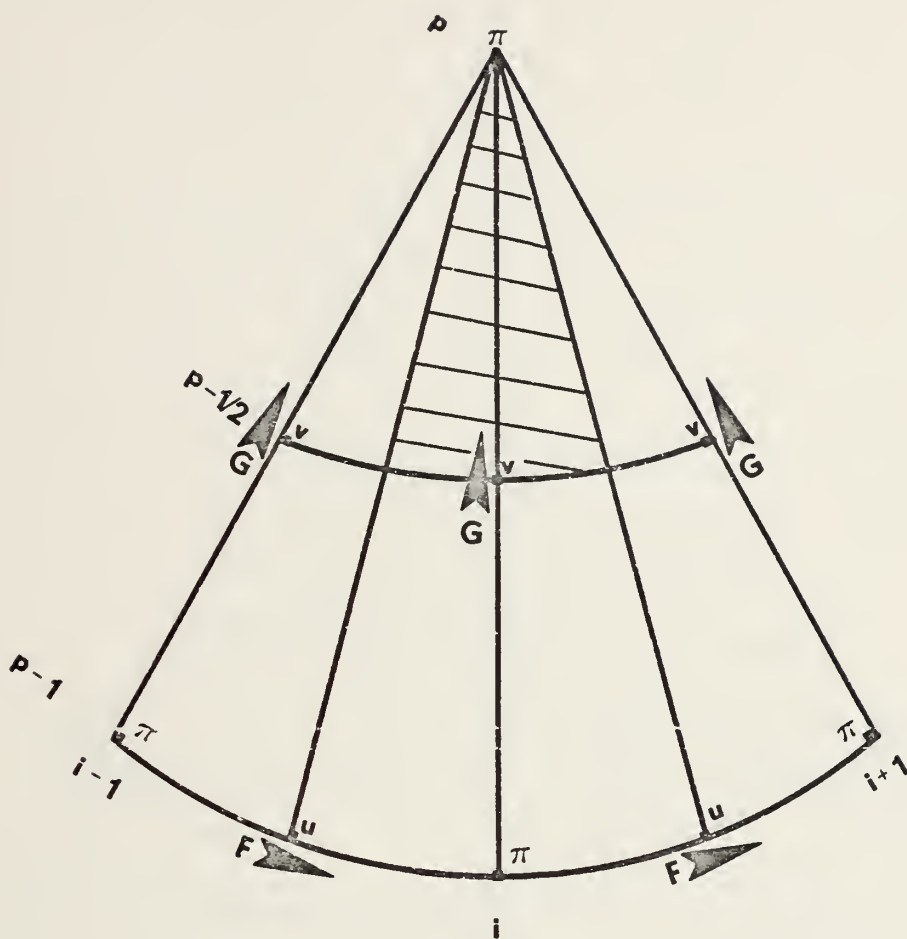


Figure 8. Each index  $i, P$  in the continuity equation is represented by the shaded area.  $\pi$  at the poles can only change as a result of  $G$ . The thermodynamic equation and vertical velocity are treated in the same manner.



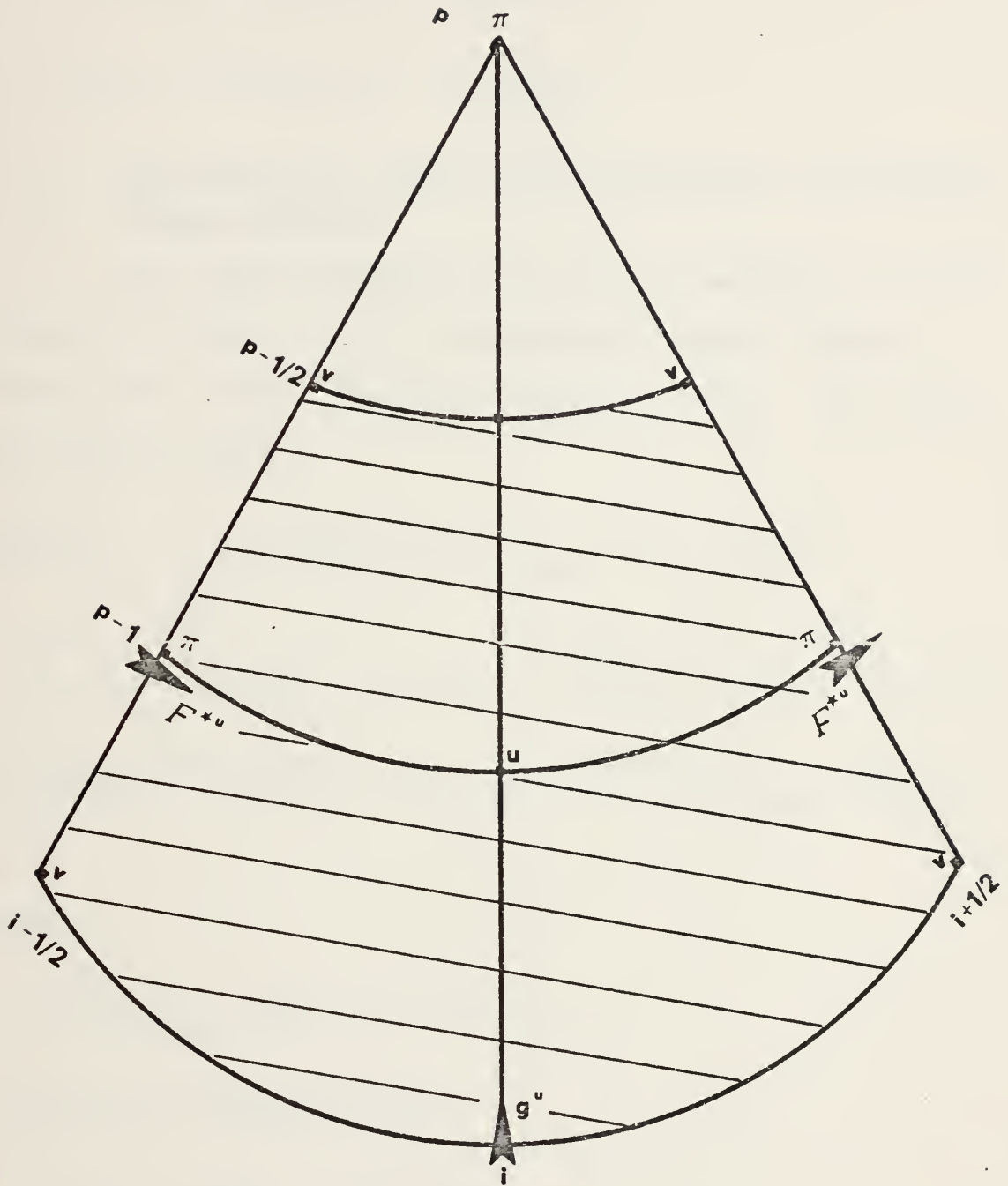


Figure 9. The polar modification of the  $u$  equation of motion.  $F^{*u}$  and  $g^u$  are flux terms. The shaded portion represents the area associated with each variable  $u$ .



$g^u$  given by equation (3.12)

$$\Pi_{i,P-1}^u \equiv \frac{1}{2}(\Pi_{i-\frac{1}{2},P-1} + \Pi_{i+\frac{1}{2},P-1}) ,$$

$$\dot{S}_{i,P-1}^u \equiv \frac{1}{2}(\dot{S}_{i-\frac{1}{2},P-1} + \dot{S}_{i+\frac{1}{2},P-1}) .$$

## 2. The Advective Terms in the $\eta$ -component of the Equation of Motion

The polar modification of the  $\eta$ -component is represented in figure 10. It was modified from the Arakawa scheme in a similar manner as equation (3.22). The following form is used:

$$\begin{aligned} & \frac{\partial(\Pi_{v,k}^v)}{\partial t}_{i,P-\frac{1}{2}} + \frac{1}{2}[F_{i+\frac{1}{2},P-\frac{1}{2}}^{*v}(v_{i+1,P-\frac{1}{2}} + v_{i,P-\frac{1}{2}})^k \\ & - F_{i-\frac{1}{2},P-\frac{1}{2}}^{*v}(v_{i,P-\frac{1}{2}} + v_{i-1,P-\frac{1}{2}})^k - g_{i,P-1}^v(v_{i,P-\frac{1}{2}} + v_{i,P-\frac{3}{2}})^k] \\ & + \frac{1}{\Delta\sigma^k} \frac{1}{2}[\dot{S}^{v,k+1}(v_{i,P-\frac{1}{2}}^{k+2} + v_{i,P-\frac{1}{2}}^k) - \dot{S}^{v,k-1}(v_{i,P-\frac{1}{2}}^k + v_{i,P-\frac{1}{2}}^{k-2})] , \end{aligned} \quad (3.23)$$

where

$$F_{i-\frac{1}{2},P-\frac{1}{2}}^{*v} \equiv \frac{1}{4}(F_{i-1,P-1}^* + F_{i,P-1}^*),$$

$g^v$  given by equation (3.16),

$$\Pi_{i,P-\frac{1}{2}}^v \equiv \frac{1}{2}(\Pi_{i,P} + \Pi_{i,P-1}) ,$$

$$\dot{S}_{i,P-\frac{1}{2}}^v \equiv \frac{1}{2}(\dot{S}_{i,P} + \dot{S}_{i,P-1}) .$$





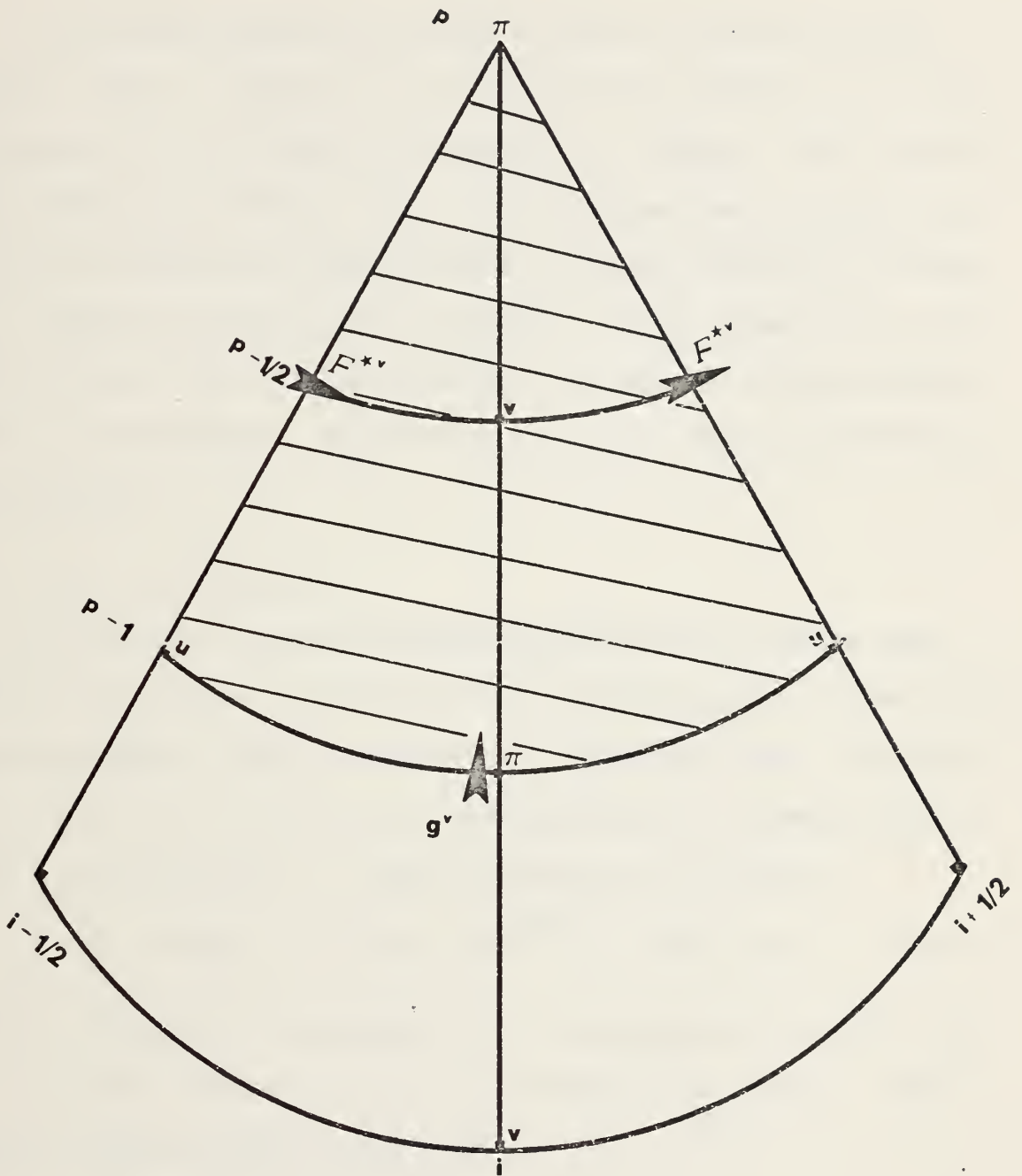


Figure 10. The polar modification of the  $v$  equation of motion.  $F^{*v}$  and  $g^{*v}$  are flux terms. The shaded portion represents the area associated with each variable  $v$ .



#### IV. ANALYTIC INITIALIZATION

The initial conditions were similar to those used by Maher (1974). Analytic initial conditions offer several advantages in the initial evaluation of a model; they simplify the otherwise difficult task of balancing and interpolating initial conditions from constant pressure surfaces to sigma ( $\sigma$ ) surfaces, they allow the angular phase speed to be estimated from a non-divergent model and they allow the simulation of atmospheric states that otherwise would be difficult to simulate.

##### A. ANALYTIC BALANCING

The initial terrain pressure and velocity fields were obtained from the stream function solution to the linearized, non-divergent vorticity equation (Haurwitz, 1940). The complete vorticity equation was later solved by Neamtan (1946). The stream function,  $\psi$ , may be written as follows:

$$\psi = A \sin(m_k \lambda - vt) \sin \phi \cos^{m_k} \phi - Ba^2 \sin \phi, \quad (4.1)$$

where A and B are constants,  $v$  is the angular velocity,  $m_k$  is the wave number and  $a$  is the radius of the earth. The angular phase speed is given by

$$\frac{v}{m_k} = B \frac{N(N+1) - 2}{N(N+1)} - \frac{2\Omega}{N(N+1)}, \quad (4.2)$$

where  $v/m_k$  is the angular phase speed,  $N=m_k+1$  and  $\Omega$  is the angular velocity of the earth. Harmonic waves defined by



the stream function will move with a constant angular velocity without changing shape assuming a barotropic, non-divergent atmosphere (Haurwitz, 1940). However, the equations used in this model are for a divergent atmosphere and will give a smaller contribution from the second term in the equation (4.2), especially with small wave numbers.

Equation (4.1) is used as the forcing function to obtain the geopotential from the non-linear balance equation (Phillips, 1959). The geopotential perturbation,  $\phi'$ , may be written

$$\phi' = a^2 A(\phi) + a^2 B(\phi) \sin m_k \lambda + a^2 C(\phi) (2 \sin^2 m_k \lambda - 1) \quad (4.3)$$

where

$$A(\phi) = \frac{B}{2} (2\Omega + B) \cos^2 \phi + \frac{1}{4} \left( \frac{A}{a^2} \right)^2 \cos^{2m_k} \phi$$

$$\left[ (m_k + 1) \cos^2 \phi + (2m_k^2 - m_k - 2) - \frac{2m_k^2}{\cos^2 \phi} \right], \quad (4.4)$$

$$B(\phi) = \frac{2(\Omega + B) \frac{A}{a^2}}{(m_k + 1)(m_k + 2)} \cos^{m_k} \phi \left[ (m_k^2 + 2m_k + 2) \right.$$

$$\left. - (m_k + 1)^2 \cos^2 \phi \right], \quad (4.5)$$

$$C(\phi) = \frac{1}{4} \left( \frac{A}{a^2} \right)^2 \cos^{2m_k} \phi \left[ (m_k + 1) \cos^2 \phi - (m_k + 2) \right]. \quad (4.6)$$



## B. ANALYTIC WINDS

The wind components were obtained as follows:

$$u = - \frac{1}{a} \frac{\partial \psi}{\partial \phi} , \quad (4.7)$$

$$v = \frac{1}{a \cos \phi} \frac{\partial \psi}{\partial \lambda} . \quad (4.8)$$

Performing the operations indicated above the  $u$  and  $v$  components may be written

$$u = - \frac{1}{a} [A \sin(m_k \lambda - vt) \cos^{m_k+1} \phi - m_k A \sin(m_k \lambda - vt) \cos^{m_k-1} \phi \sin^2 \phi - B a^2 \cos \phi] , \quad (4.9)$$

$$v = \frac{1}{a} [A m_k \sin \phi \cos^{m_k-1} \phi \cos (m_k \lambda - vt)] . \quad (4.10)$$

## C. TEMPERATURE

The temperature field was derived in accordance with the NACA standard atmosphere as follows (Haltiner and Martin, 1957):

$$T(^{\circ}\text{K}) = 288 - 0.0065Z, \quad (4.11)$$

$$Z \text{ (meters)} = 44308 \left[ 1 - \left( \frac{p}{1013.25} \right)^{0.19023} \right] , \quad (4.12)$$

where  $Z \leq 10769$  meters.





## V. MODEL PERFORMANCE

The evaluation of the model was a two-step process. The first step involved the use of a coarse grid and was essentially a scheme to minimize computer time while debugging. The second step involved the use of a finer grid for better resolution. The majority of the experiments presented in this chapter were run with the fine grid.

The coarse grid consisted of 16 points N-S which gave a 12 degree separation between grid points. Since strictly analytic initial conditions were used it was only necessary to integrate over one wave using cyclic continuity and therefore a 10-point E-W grid was adequate. The E-W grid distance was a function of wave number. Wave numbers 4, 8 and 12 were used in the experiments. Wave number 4 gave an E-W grid spacing of 9 degrees, wave number 8 gave a grid spacing of 4.5 degrees and wave number 12 gave a grid spacing of 3 degrees. The fine grid used 46-points N-S which gave a grid spacing of 4 degrees. The E-W grid was similar to the coarse grid.

In all cases the model was run with two levels, a flat earth and no source or sink terms. The time step ( $\Delta t$ ) was six minutes. Fourier analysis of the surface pressure field was used to compute phase speed and wave amplitude in all but experiment III in which a Fourier analysis of the wind field was computed. Calcomp charts were plotted at 12 hour



intervals and consisted of one wave of the surface pressure field over the complete N-S grid. The phase speed and wave amplitude were initialized through the constants A and B given in equation (4.1), where A is the amplitude of the disturbance and B is the amplitude of the mean flow.

Experiment I. Wave numbers 4, 8 and 12 were used to determine the phase speed over the coarse, 16-point grid. The phase speed was set at 10 degrees per day by adjusting the amplitude of the mean flow (B). The graphs of phase angle (degrees longitude) vs latitude are shown in figures 11, 12 and 13. The observed phase speed approached 20 degrees over 48 hours for all three cases.

Experiment II. This and all subsequent experiments were run over the 46-point N-S grid. External gravity waves were simulated with wave number 4 by setting the mean flow, the u and v components of the wind and the Coriolis terms to zero. The theoretical period of the gravity wave was calculated using the following approximation:

$$T_p = \frac{2(3.14159)}{C K_p}, \quad (5.1)$$

where

$$K_p = \frac{\sqrt{N(N+1)}}{a}.$$

C is the zonal phase speed (set at 300 m/sec),  $K_p$  is the two-dimensional wave number,  $N=m_k+1$ , a is the radius of the earth and  $T_p$  is the period. The above approximation gives a



period on the order of 7 hours for wave number 4. The observed oscillations of the surface pressure field as a function of time are given in figure 14. The period is on the order of 6-7 hours.

Experiment III. In this experiment pure advection was simulated with wave number 4 by removing the Coriolis terms, the pressure gradient terms and the vertical advection terms. The surface pressure and the temperature were kept constant. The u and v components of the wind were Fourier analyzed to determine phase angle and amplitude. The theoretical advection was determined by taking the mean zonal component of the wind ( $\bar{u}$ ) over a given time period. A percentage of the actual advection/theoretical advection vs latitude for a 6-hour period is shown in figure 15.

Experiment IV. This experiment was designed to analyze the  $\beta$  effect as given in equation (4.2). It can be shown that the  $\beta$  effect is represented by the last term in equation (4.2). The mean flow, B in equation (4.2), was set to zero which eliminates the large N-S pressure variation. The  $\beta$  effect is most pronounced for low wave numbers. Wave numbers 4, 8 and 12 were run. According to equation (4.2) with B set to zero, wave number 4 should retrogress at 24 degrees per day, wave number 8 should retrogress at 8 degrees per day and wave number 12 should retrogress at 4 degrees per day. The observed retrogressions are shown in figures 16, 17 and 18. The actual retrogressions were somewhat less than expected due to the mean divergence which reduces the



magnitude of  $\beta$ . The analyzed and 48-hour forecast surface pressure fields are shown in charts A through F.

Experiment V. Wave numbers 4, 8 and 12 were run with the mean flow adjusted to give a phase speed of 10 degrees per day. As the wave number increases the second term in equation (4.2) has less contribution and the phase speed approaches the initialized phase speed. Figures 19, 21 and 23 show the observed phase angle vs latitude for wave numbers 4, 8 and 12 respectively. As expected, the phase speed increased as wave number increased. The wave amplitude vs latitude are shown in figures 20, 22 and 24. In all three cases the wave form remained essentially constant over the 48-hour forecast period. The analyzed and forecast surface pressure fields are shown in charts G through L.





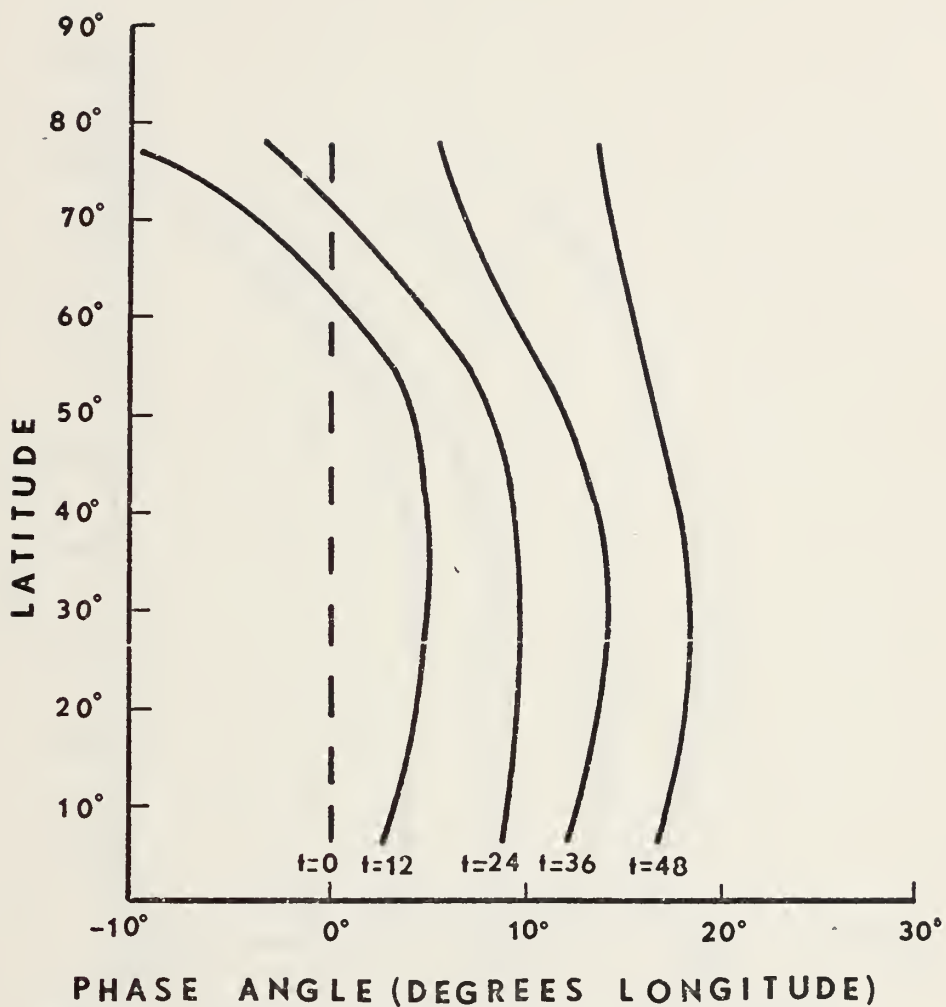


Figure 11. Phase angle (degrees longitude) vs latitude, for 16-point N-S grid, wave number 4, phase speed  $10^\circ/\text{day}$  and  $A = 7.0 \times 10^7$ . (Latitudes with zero wave amplitude are not included and time is given in hours.)



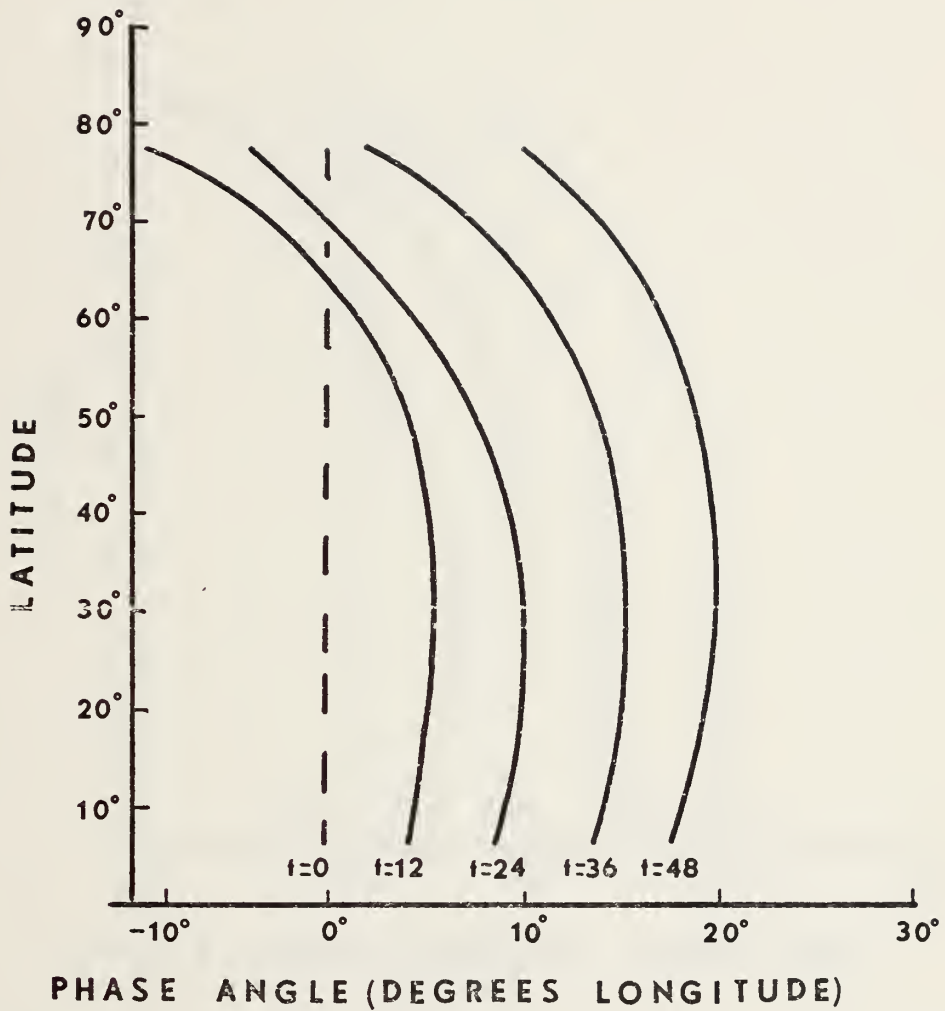


Figure 12. Phase angle (degrees longitude) vs latitude for 16-point N-S grid, wave number 8, phase speed  $10^\circ/\text{day}$  and  $A = 1.6 \times 10^8$ . (Latitudes with zero wave amplitude are not included and time is given in hours.)



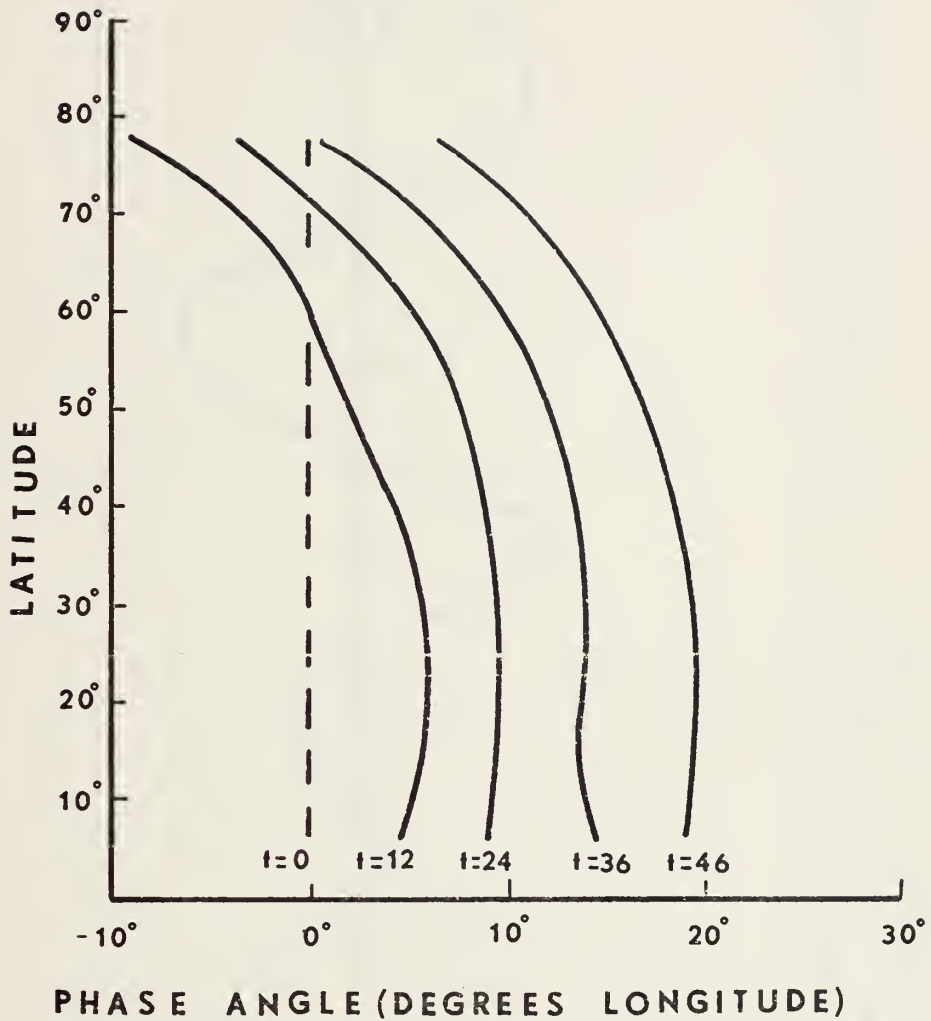


Figure 13. Phase angle (degrees longitude) vs latitude for 16-point N-S grid, wave number 12, phase speed  $10^\circ/\text{day}$  and  $A = 7.0 \times 10^7$ . (Latitudes with zero wave amplitude are not included and time is given in hours.)



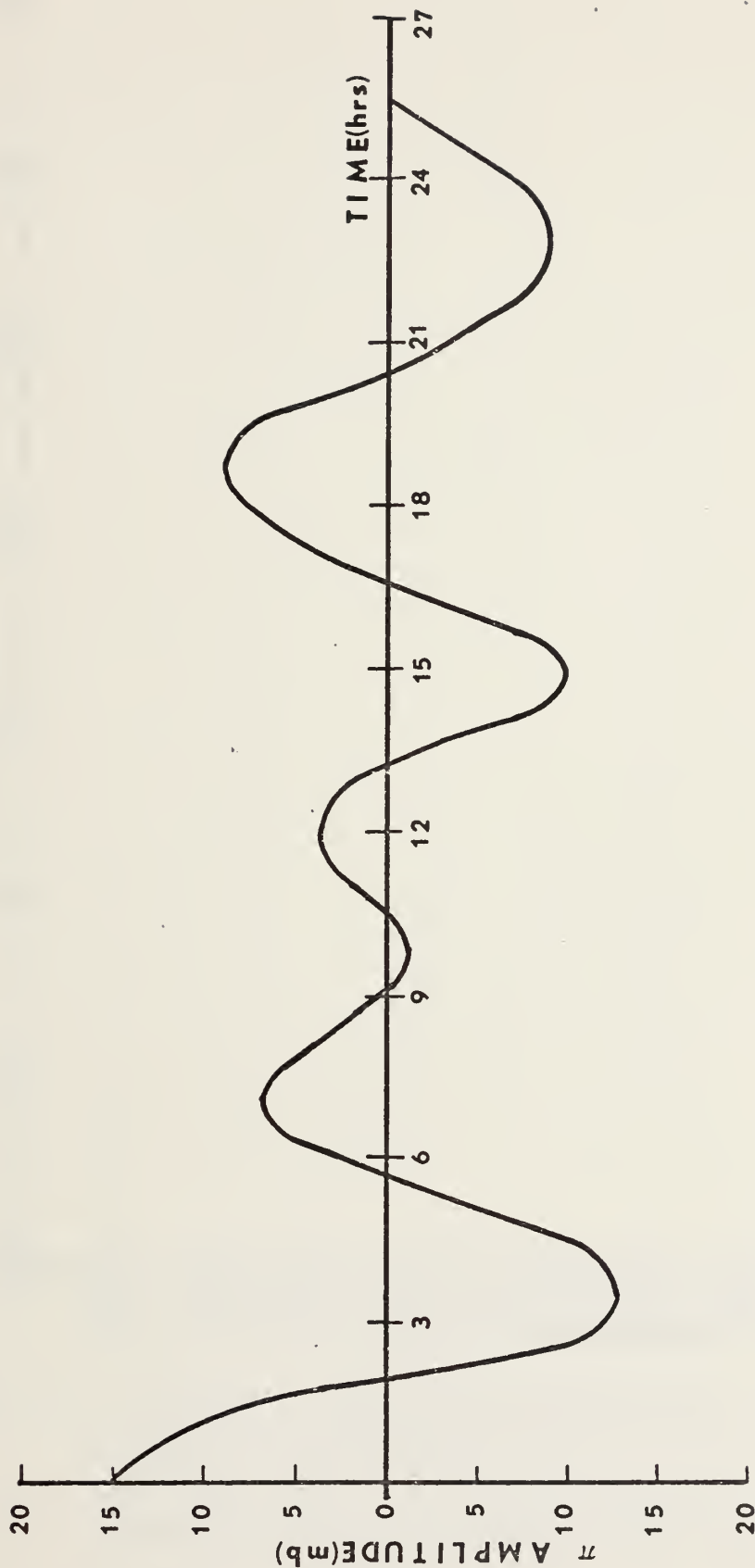


Figure 14. Terrain pressure amplitude vs time (hrs) for gravity wave oscillations, wave number 4, B (mean flow) = 0, u and v components of the wind = 0, Coriolis = 0 and  $A = 7.0 \times 10^7$ .





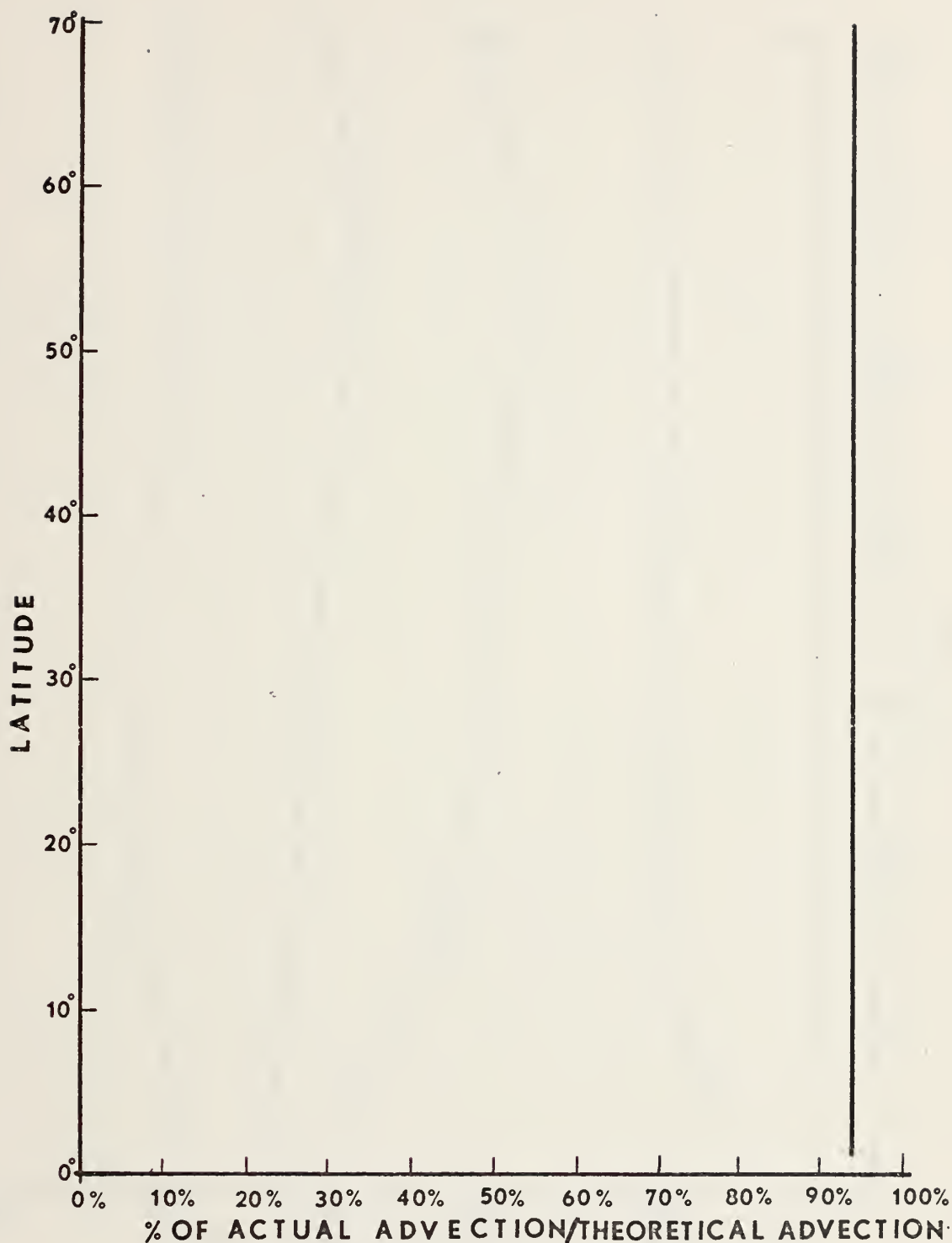


Figure 15. Percentage of actual advection/theoretical advection vs latitude for wave number 4 with  $A = 7.0 \times 10^7$ , phase speed  $10^\circ/\text{day}$ , Coriolis = 0, pressure gradient = 0, vertical advection = 0 and terrain pressure and temperature constant.



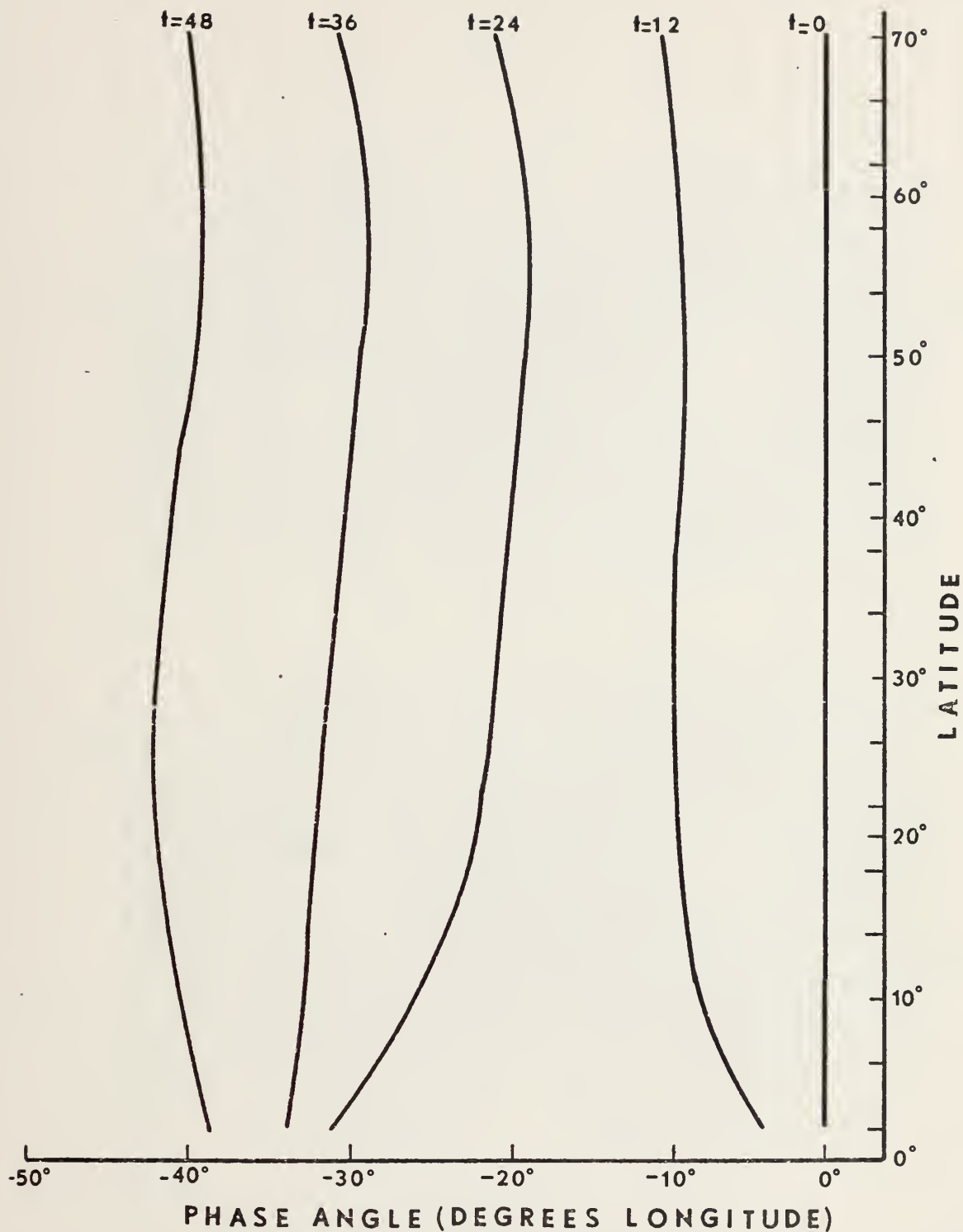


Figure 16. Phase angle (degrees longitude) vs latitude for 46-point N-S grid, wave number 4, phase speed  $-24^\circ/\text{day}$ ,  $B=0$  (no mean flow) and  $A = 7.0 \times 10^7$ . (Latitudes with zero amplitude are not included and time is given in hours.)



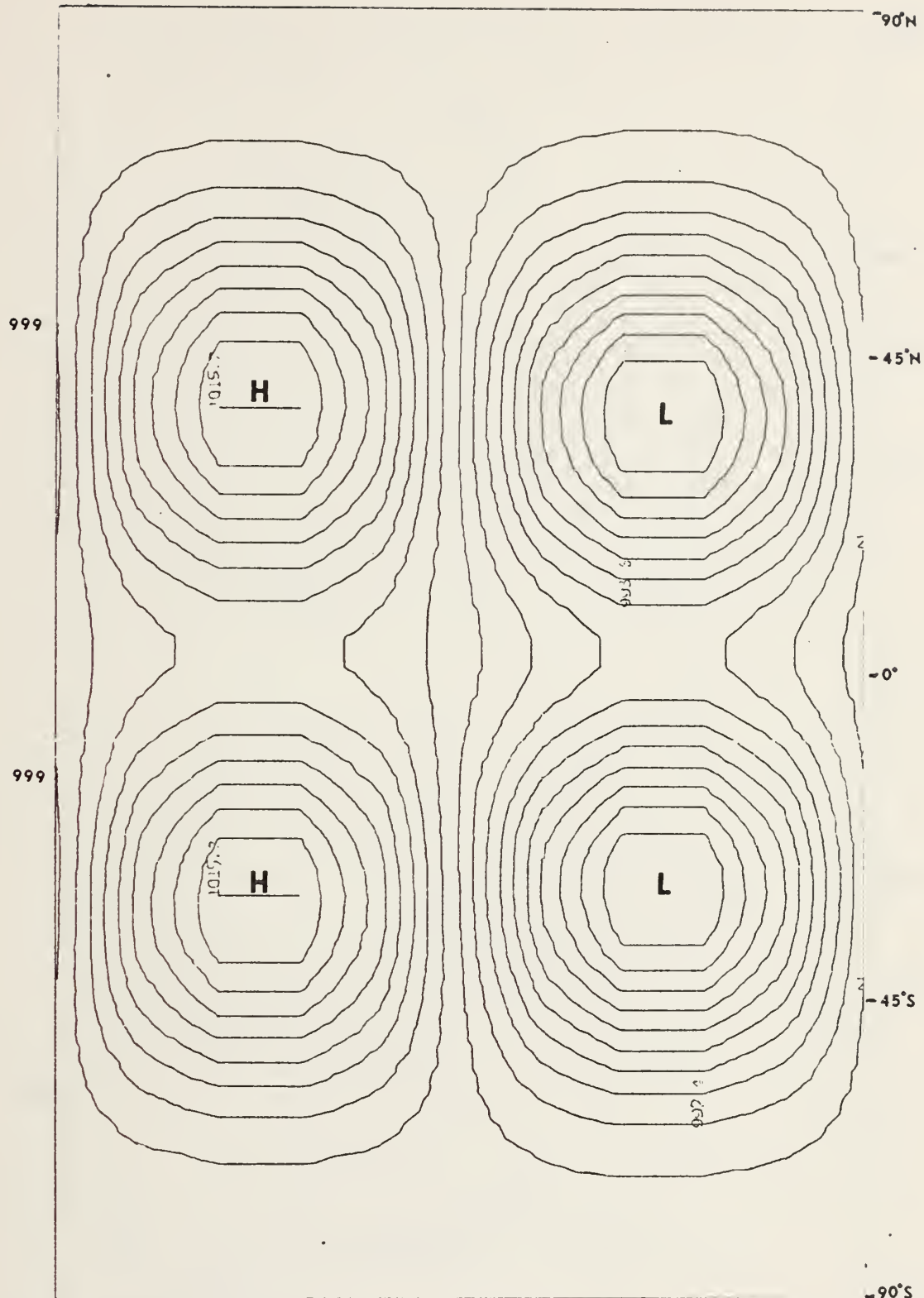


Chart A. Initial surface pressure analysis for 46-point N-S grid, wave number 4, phase speed  $-24^\circ/\text{day}$ ,  $B=0$  (no mean flow) and  $A = 7.0 \times 10^7$ .



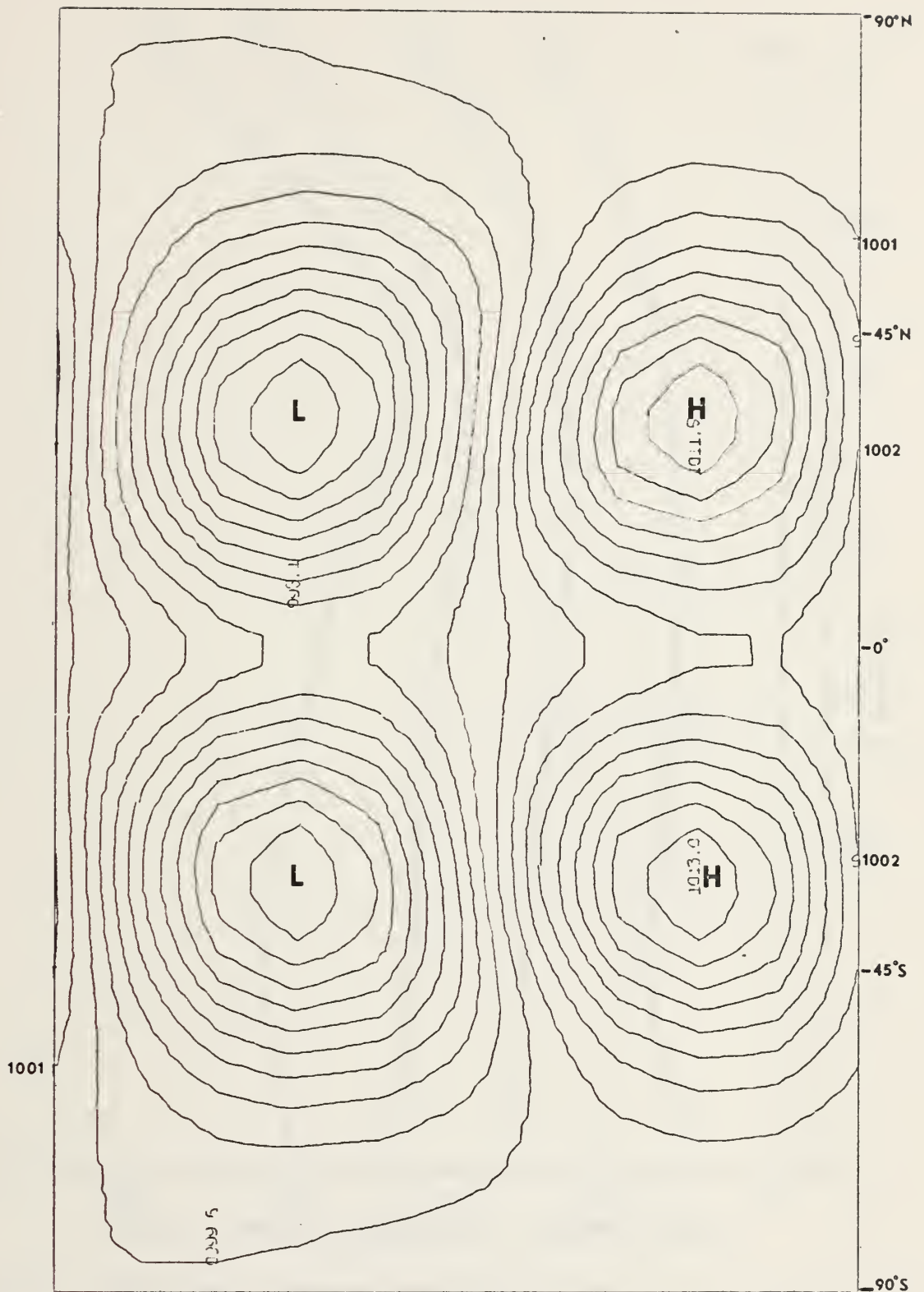


Chart B. 48-hour surface pressure forecast for 46-point N-S grid, wave number 4, phase speed  $-24^{\circ}/\text{day}$ ,  $B=0$  (no mean flow) and  $A = 7.0 \times 10^7$ .





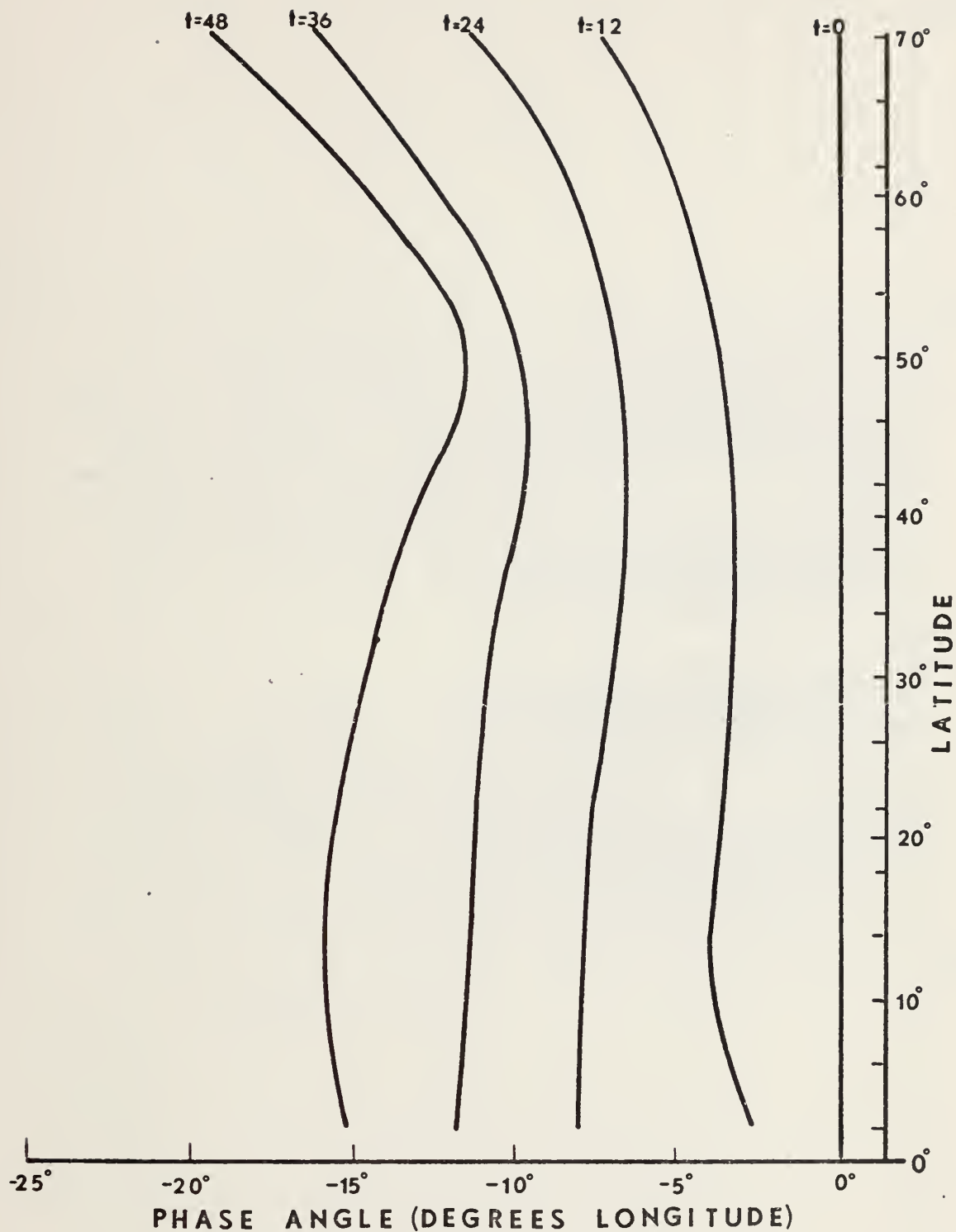


Figure 17. Phase angle (degrees longitude) vs latitude for 46-point N-S grid, wave number 8, phase speed  $-8^\circ/\text{day}$ ,  $B=0$  (no mean flow) and  $A = 1.6 \times 10^8$ . (Latitudes with zero amplitude are not included and time is given in hours.)



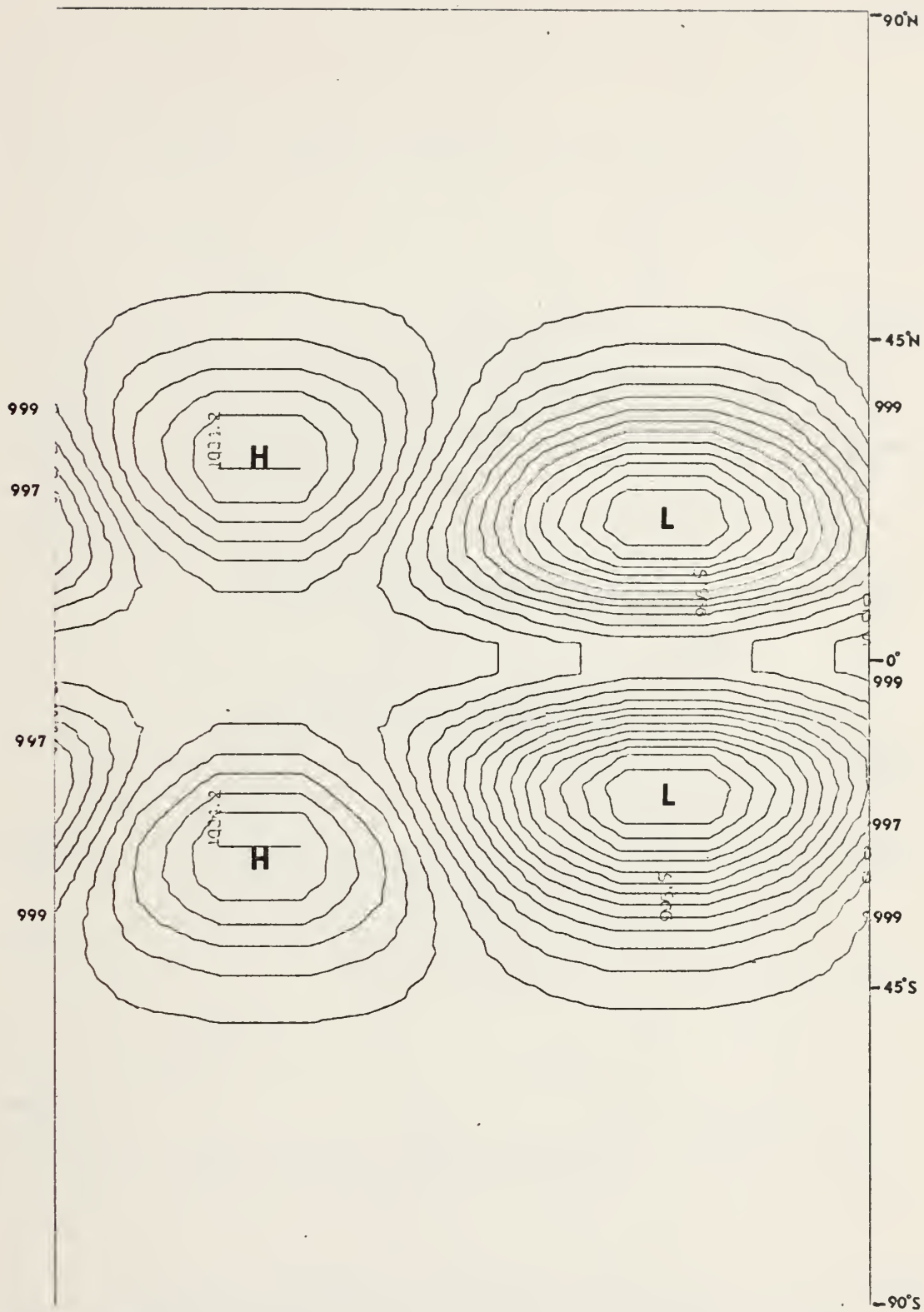


Chart C. Initial surface pressure analysis for 46-point N-S grid, wave number 8, phase speed  $-8^{\circ}/\text{day}$ ,  $B=0$  (no mean flow) and  $A = 1.6 \times 10^8$ .



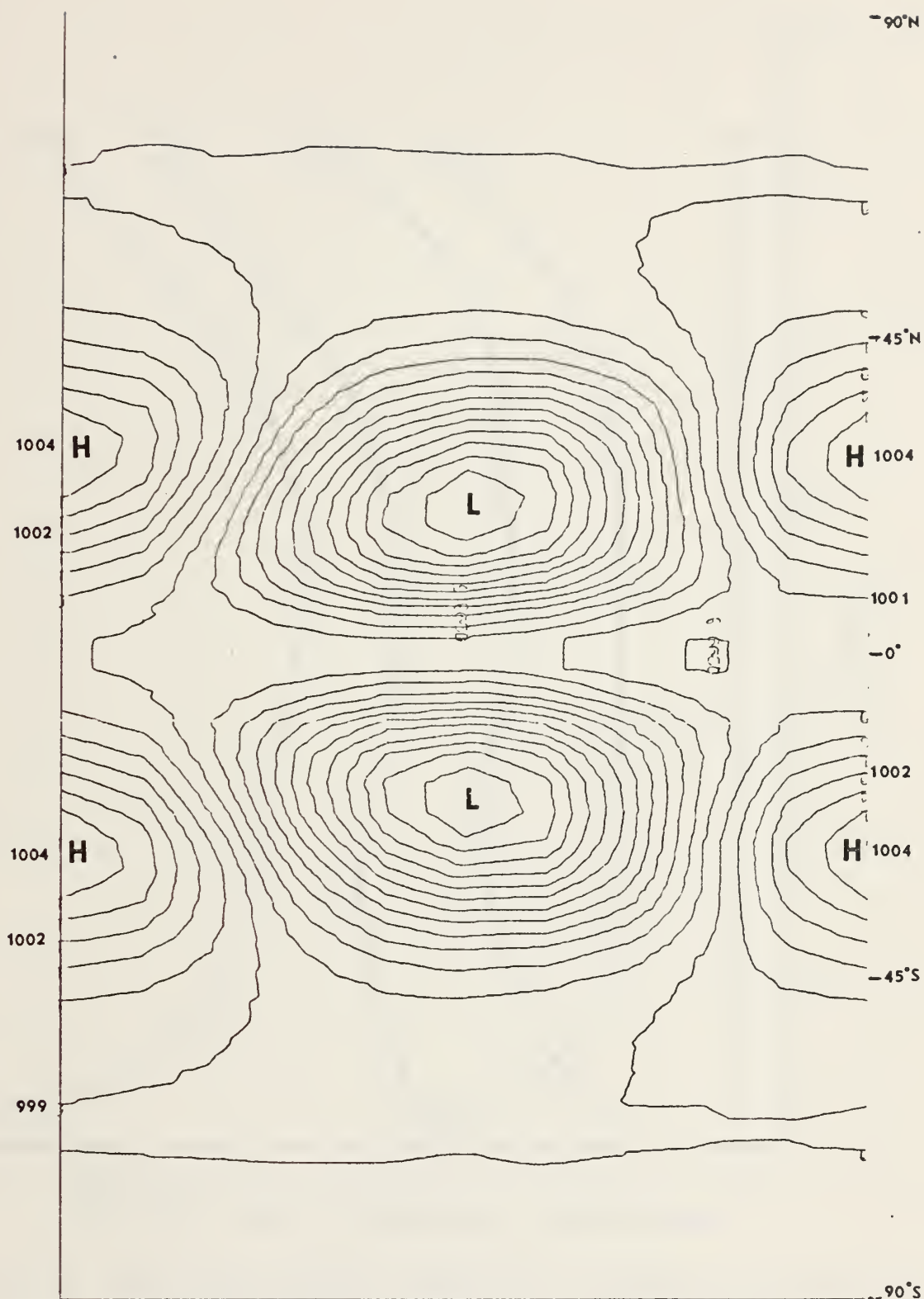


Chart D. 48-hour surface pressure forecast for 46-point N-S grid, wave number 8, phase speed  $-8^\circ/\text{day}$ ,  $B=0$  (no mean flow) and  $A = 1.6 \times 10^8$ .



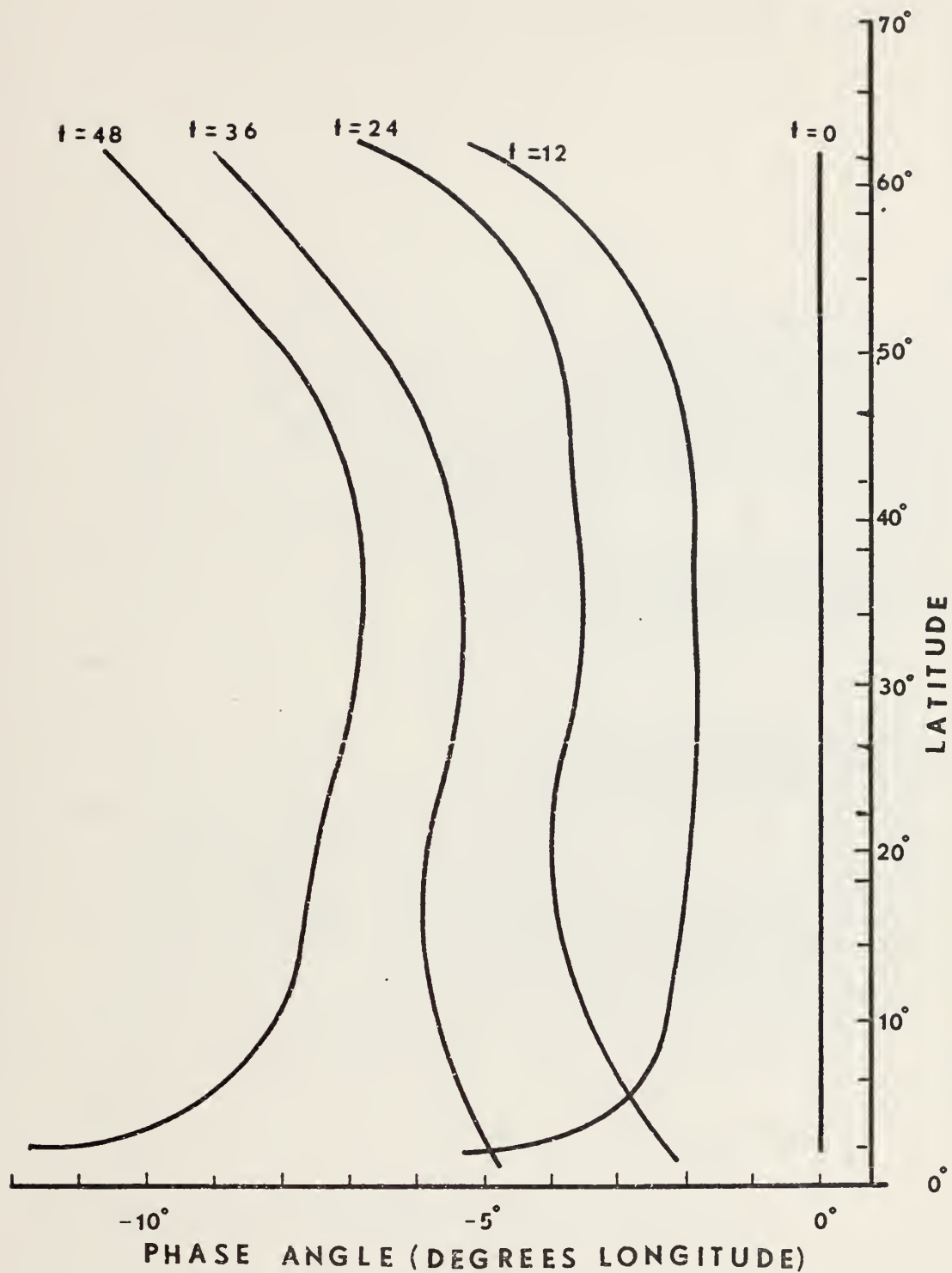


Figure 18. Phase angle (degrees longitude) vs latitude for 46-point N-S grid, wave number 12, phase speed  $-4^\circ/\text{day}$ ,  $B=0$  (no mean flow) and  $A = 7.0 \times 10^7$ . (Latitudes with zero amplitude are not included and time is given in hours.)









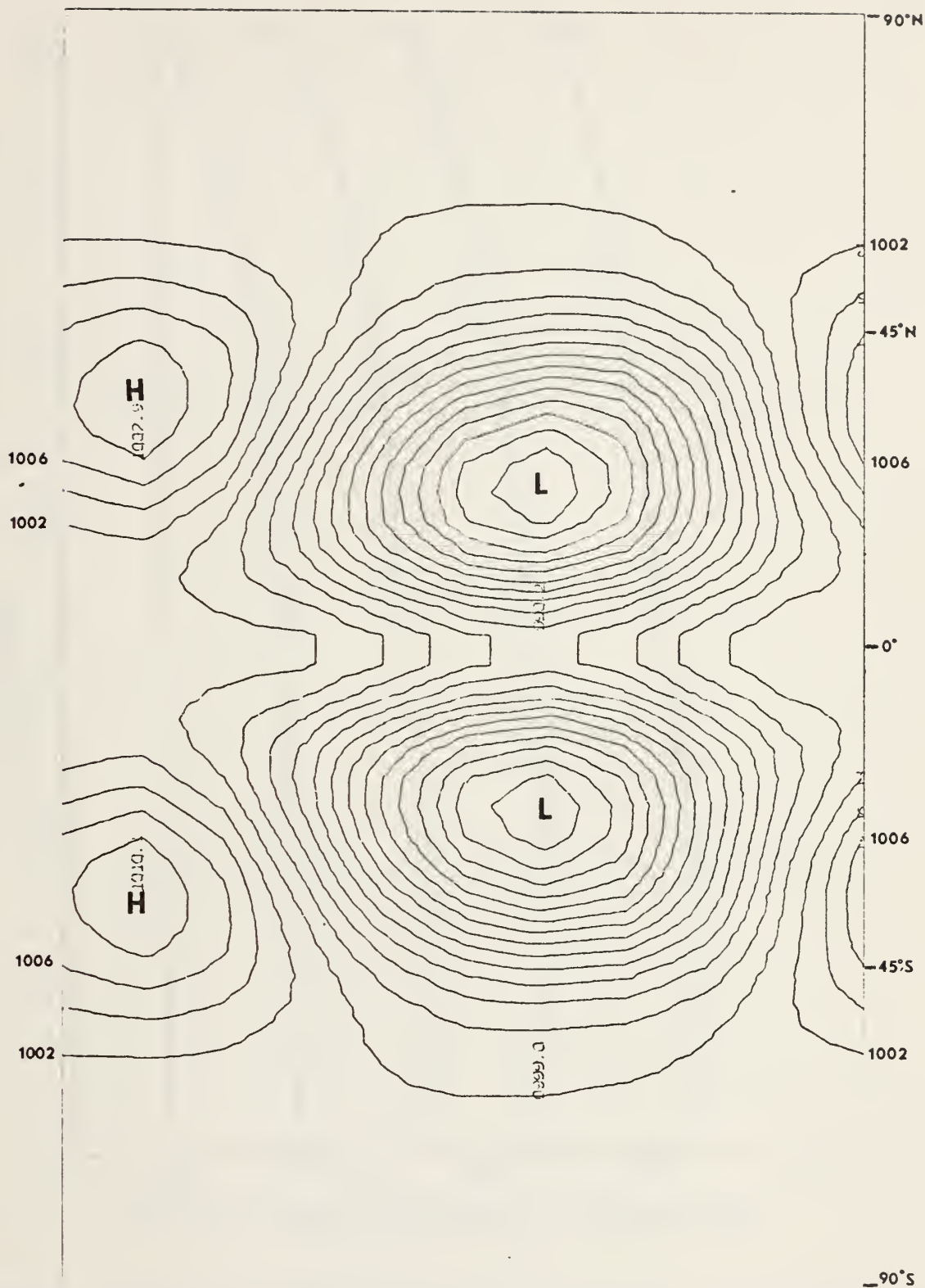


Chart F. 48-hour surface pressure forecast for 46-point N-S grid, wave number 12, phase speed  $-4^\circ/\text{day}$ ,  $B=0$  (no mean flow) and  $A = 7.0 \times 10^7$ .



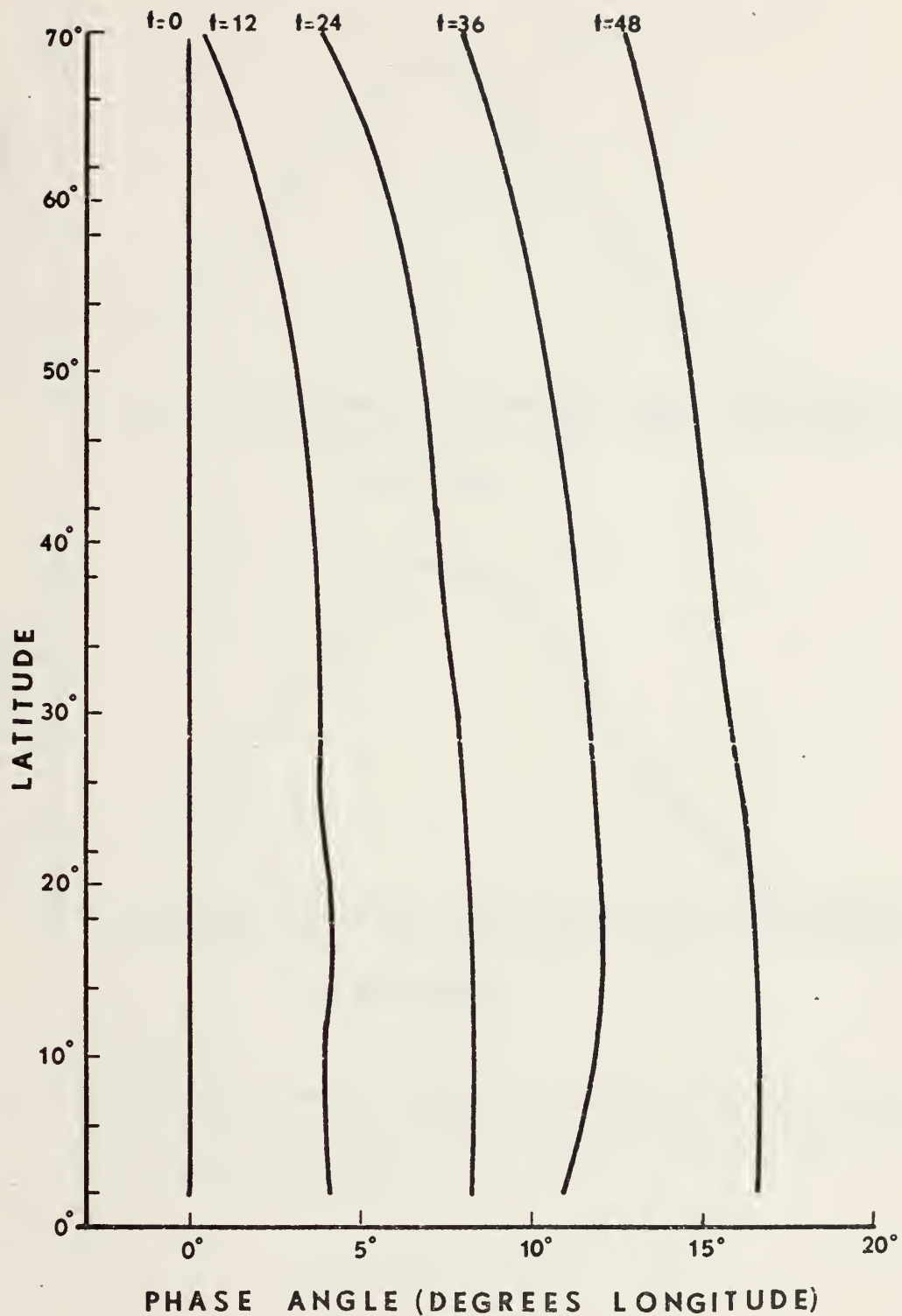


Figure 19. Phase angle (degrees longitude) vs latitude for 46-point N-S grid, wave number 4, phase speed  $10^\circ/\text{day}$  and  $A = 7.0 \times 10^7$ . (Latitudes with zero amplitude are not included and time is given in hours.)



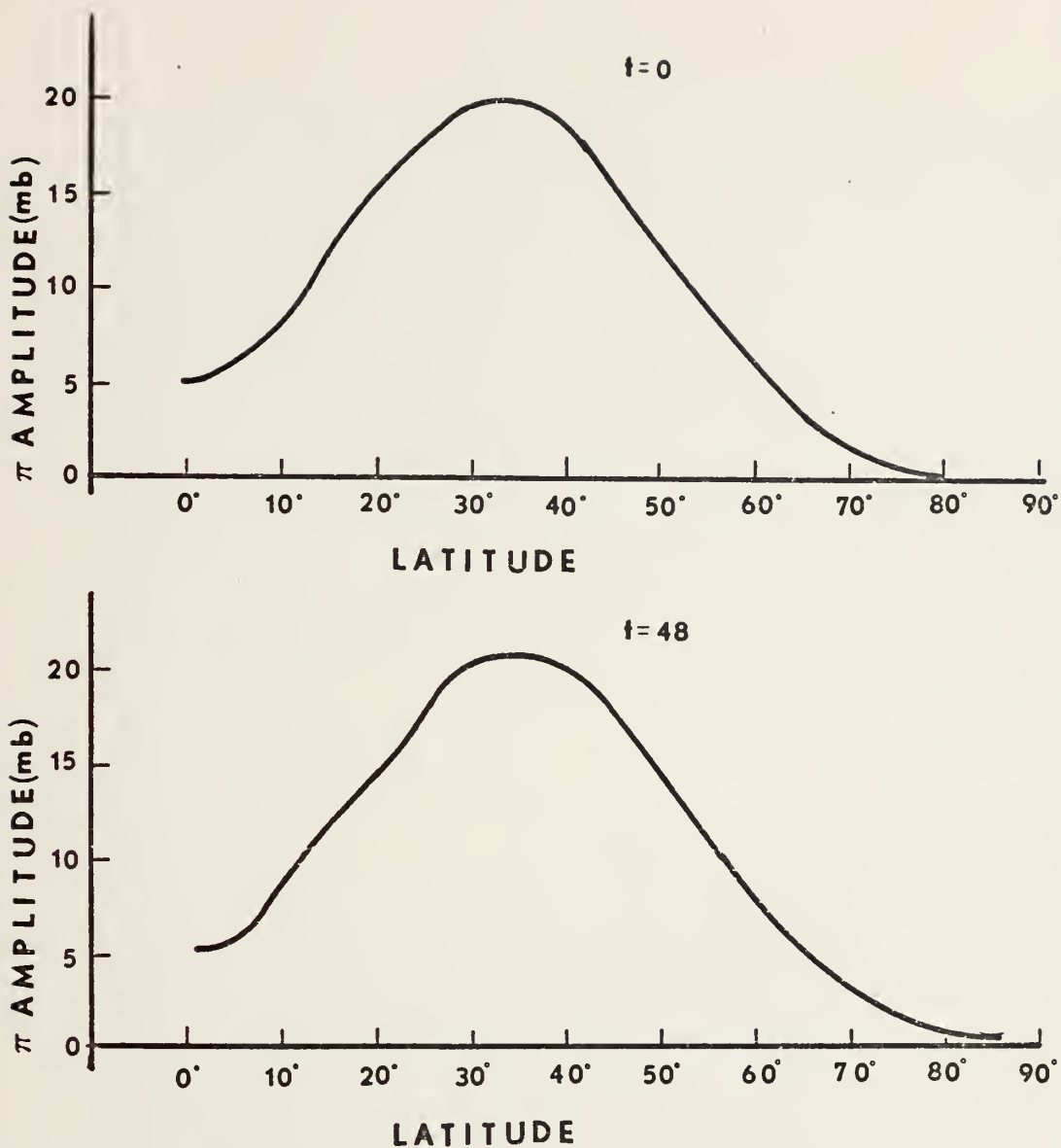


Figure 20. Terrain pressure amplitude vs latitude for initial field and 48-hour forecast, wave number 4, phase speed  $10^\circ/\text{day}$  and  $A = 7.0 \times 10^7$ .





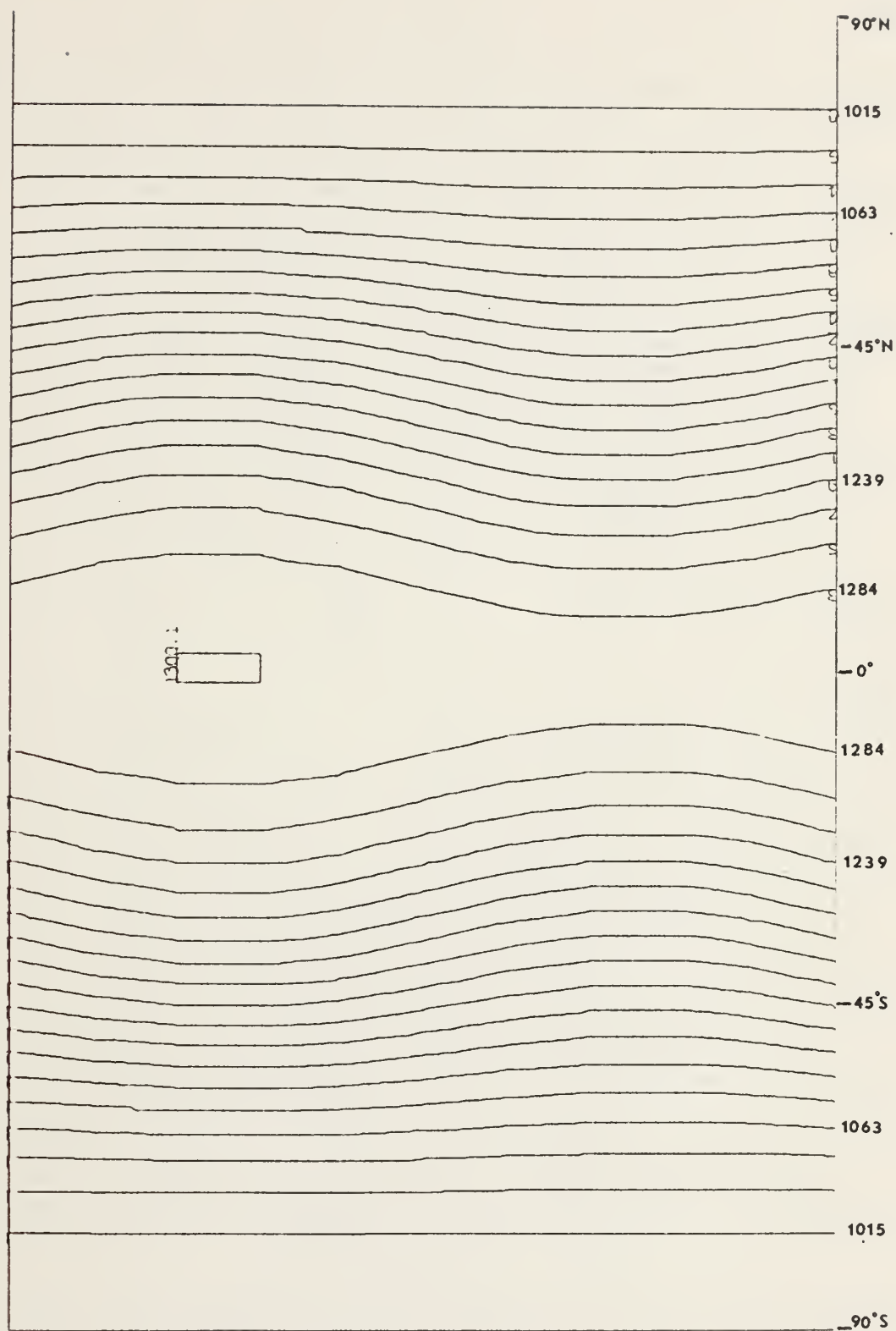


Chart G. Initial surface pressure analysis for 46-point N-S grid, wave number 4, phase speed  $10^\circ/\text{day}$  and  $A = 7.0 \times 10^7$ .



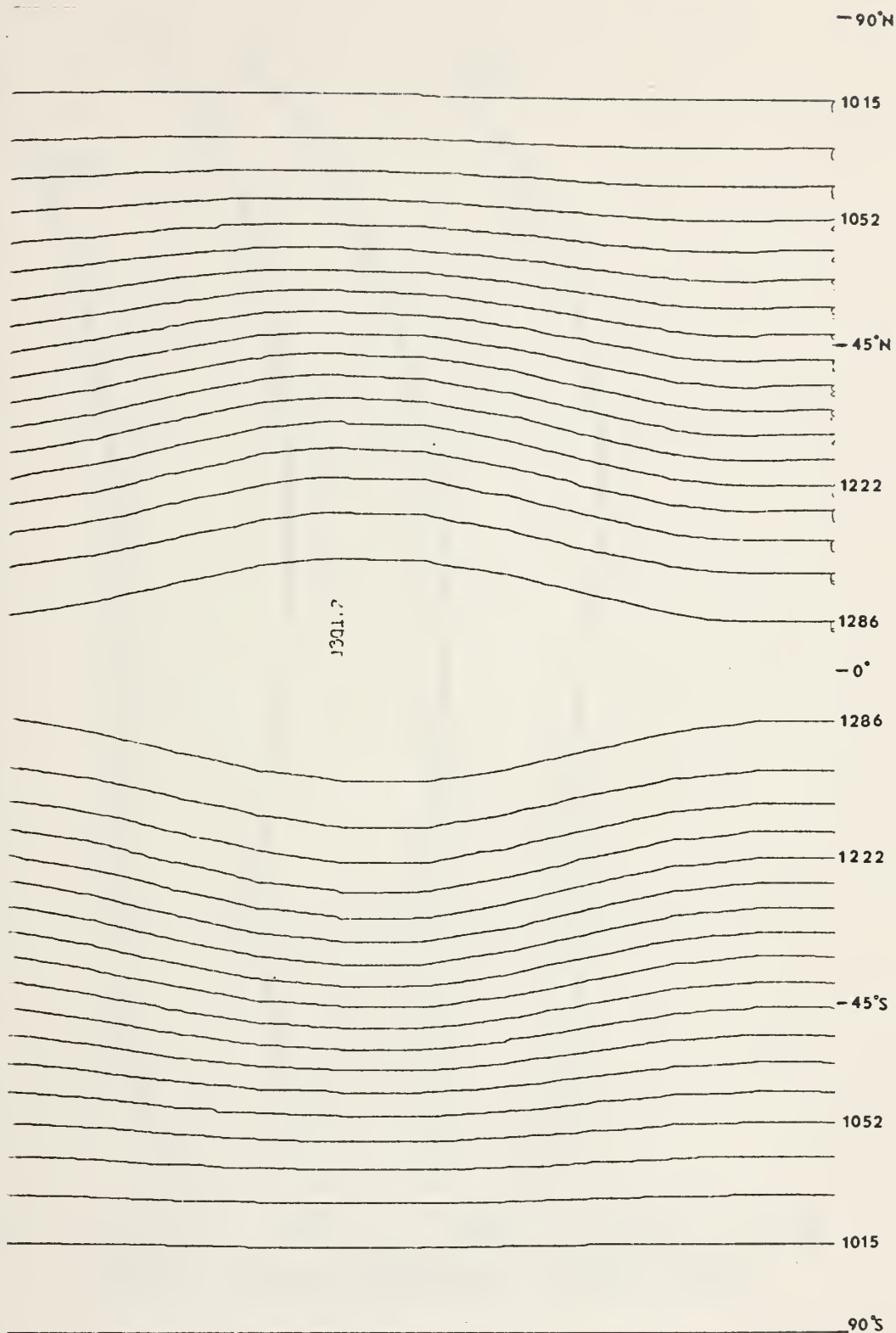


Chart H. 48-hour surface pressure forecast for 46-point N-S grid, wave number 4, phase speed  $10^\circ/\text{day}$  and  $A = 7.0 \times 10^7$ .



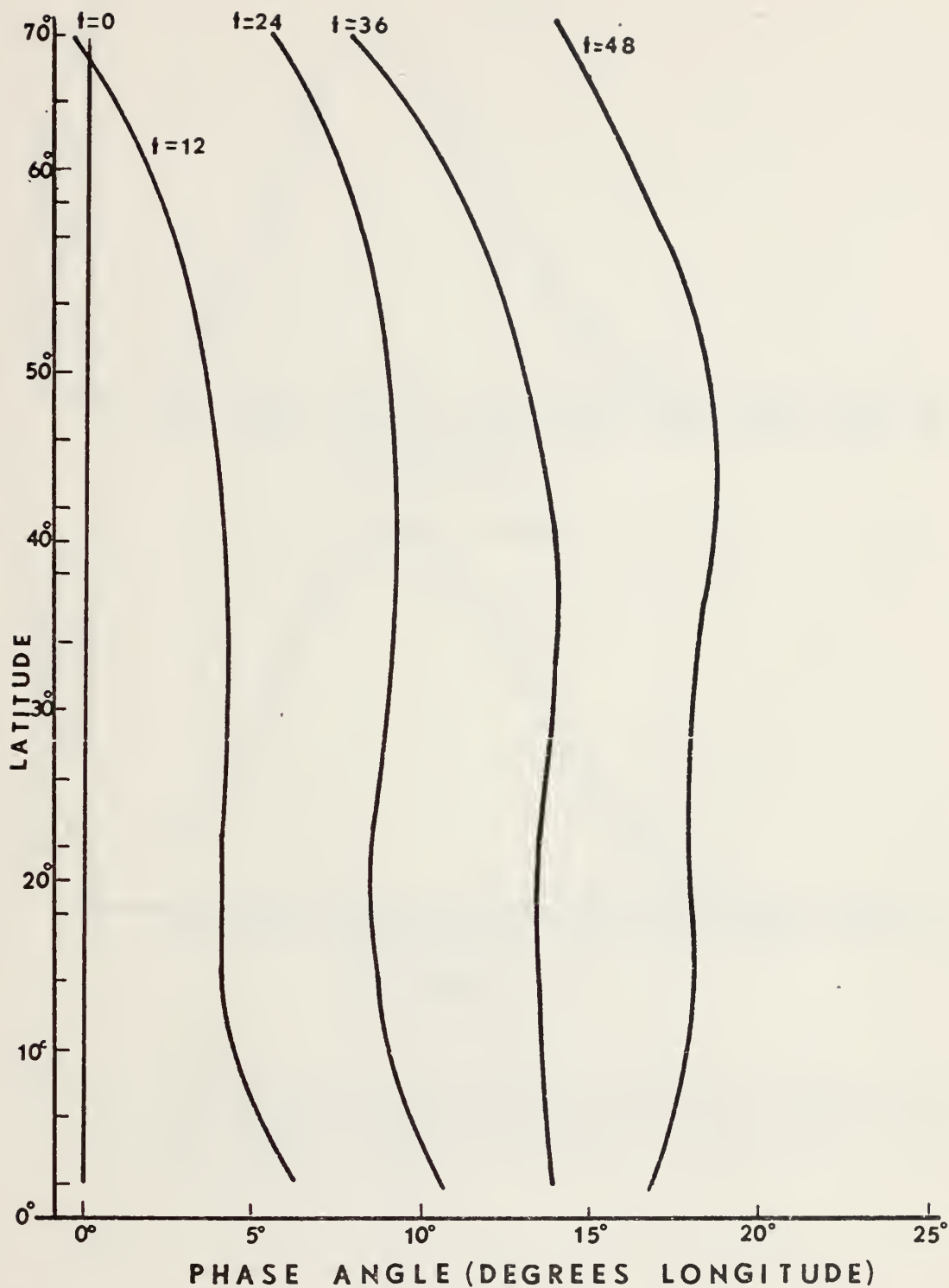


Figure 21. Phase angle (degrees longitude) vs latitude for 46-point N-S grid, wave number 8, phase speed  $10^\circ/\text{day}$  and  $A = 1.6 \times 10^8$ . (Latitudes with zero amplitude are not included and time is given in hours.)



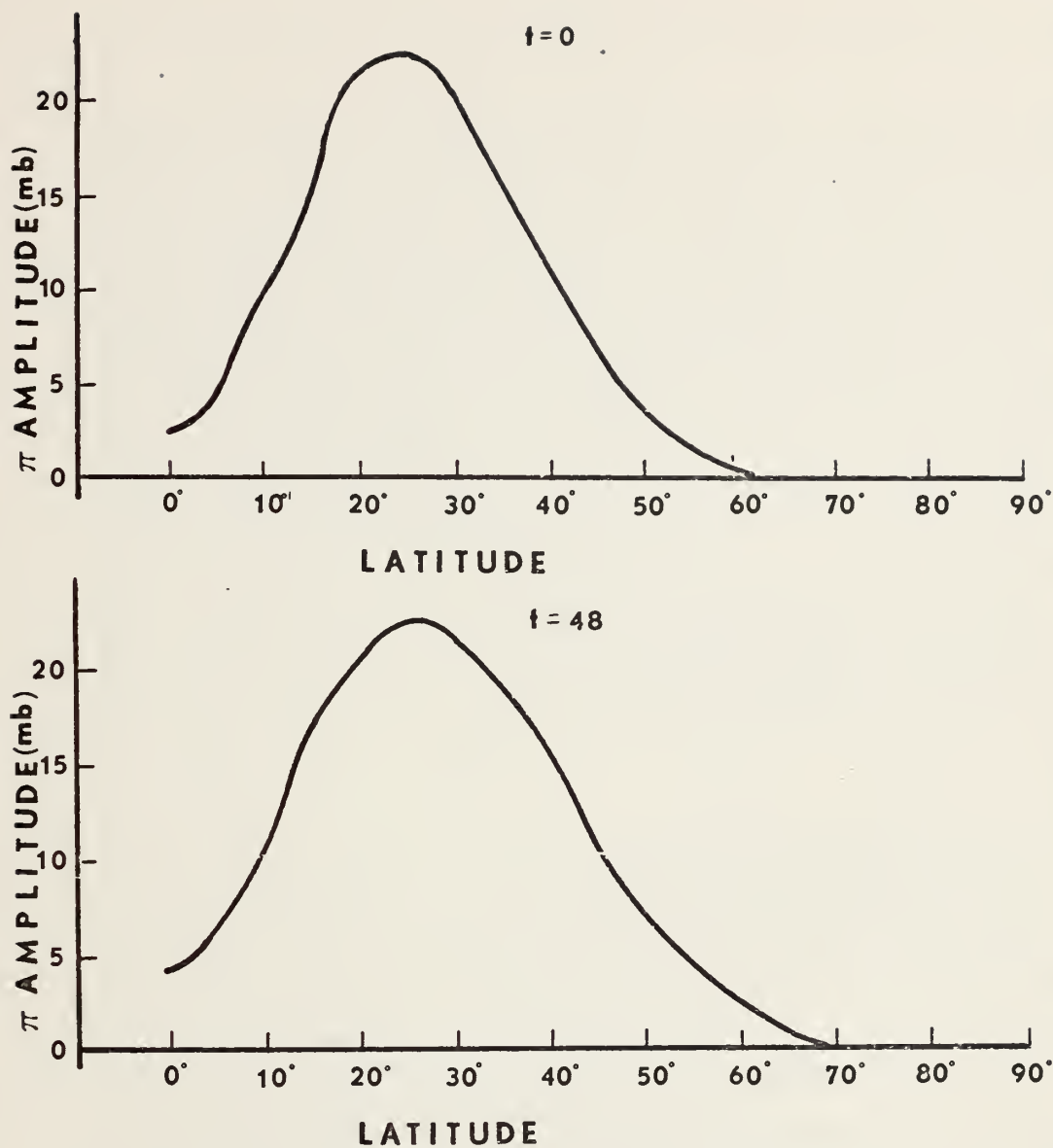


Figure 22. Terrain pressure amplitude vs latitude for initial field and 48-hour forecast, wave number 8, phase speed  $10^\circ/\text{day}$  and  $A = 1.6 \times 10^8$ .





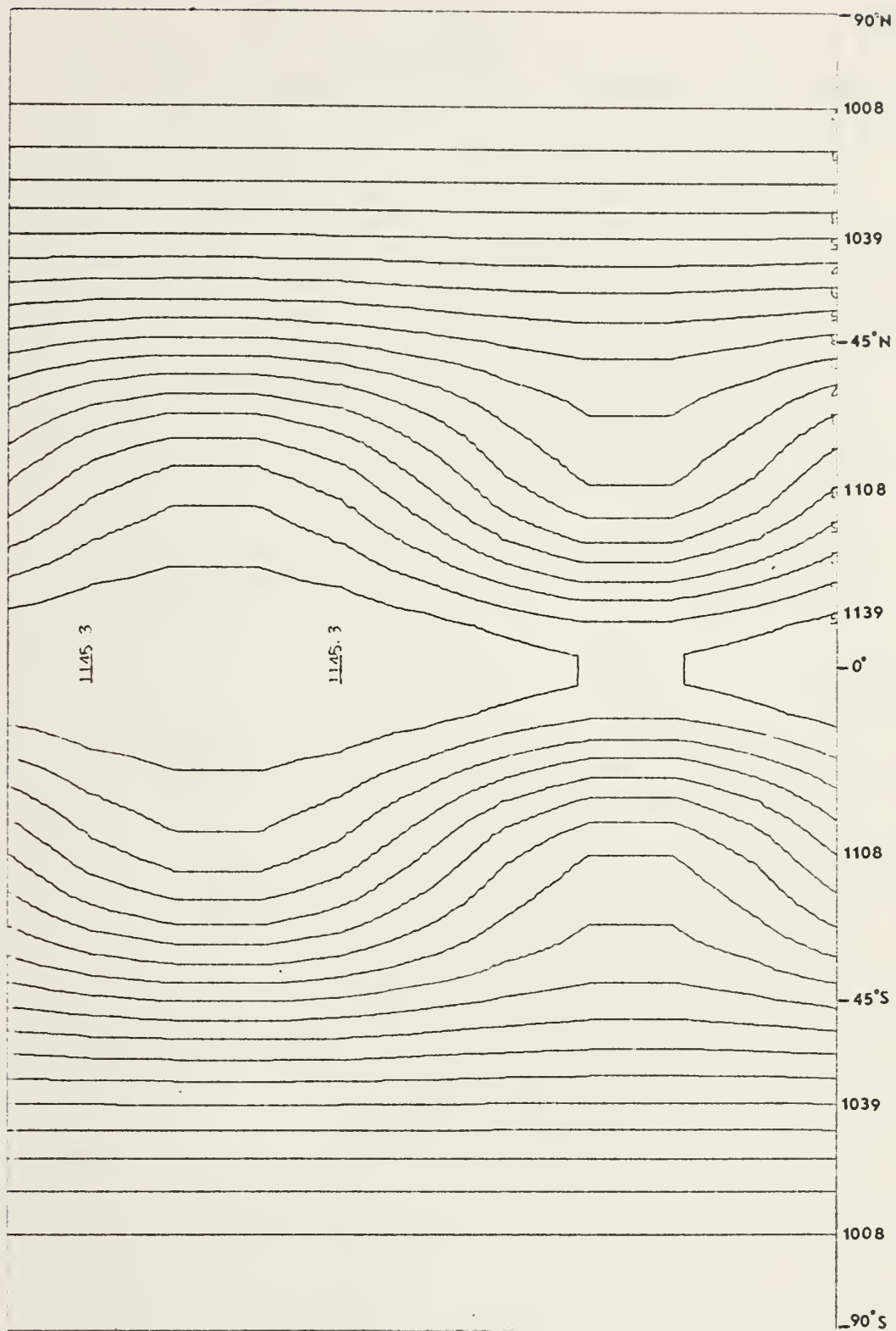


Chart I. Initial surface pressure analysis for 46-point N-S grid, wave number 8, phase speed  $10^\circ/\text{day}$  and  $A = 1.6 \times 10^8$ .



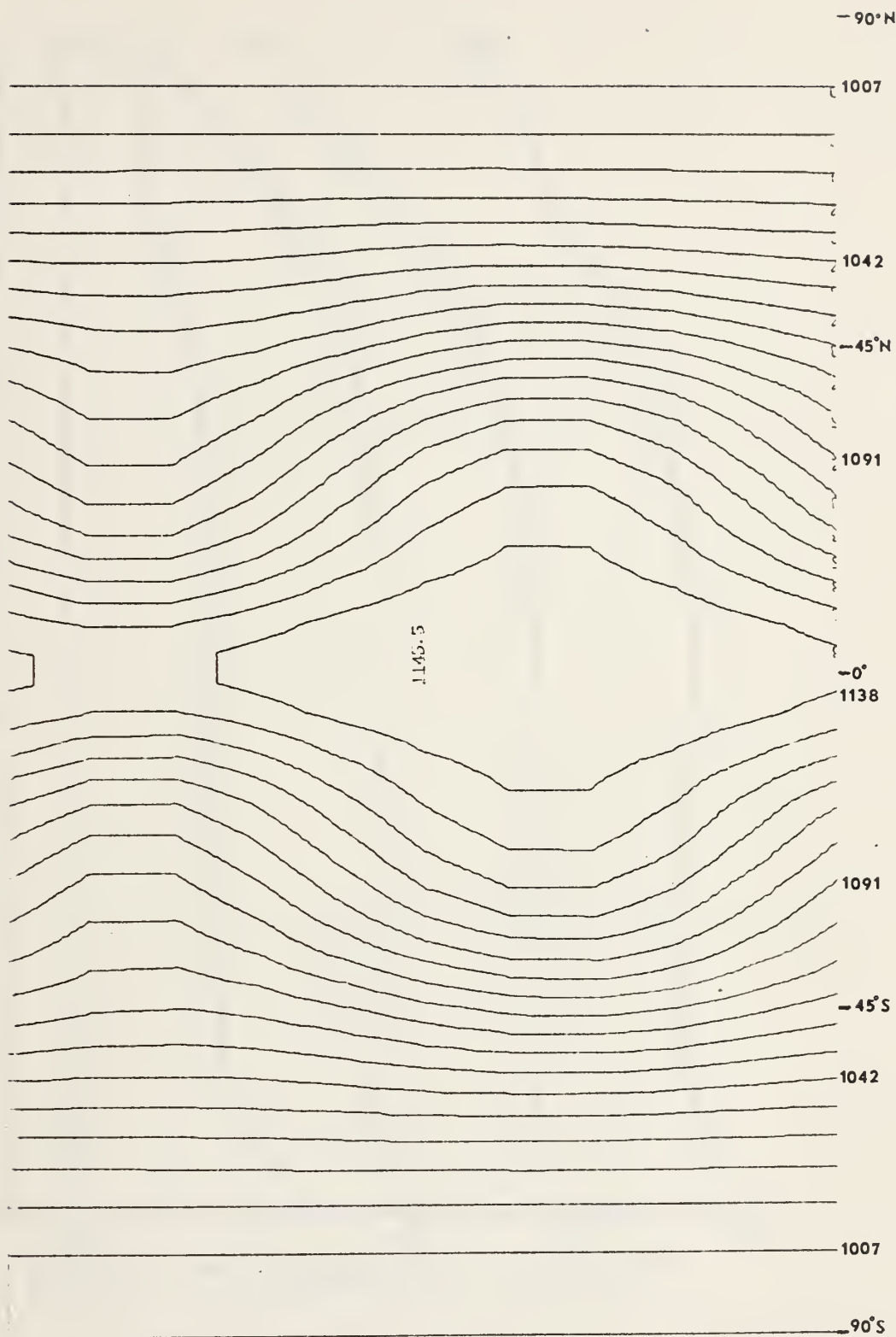


Chart J. 48-hour surface pressure forecast for 46-point N-S grid,  
wave number 8, phase speed  $10^\circ/\text{day}$  and  $A = 1.6 \times 10^8$ .



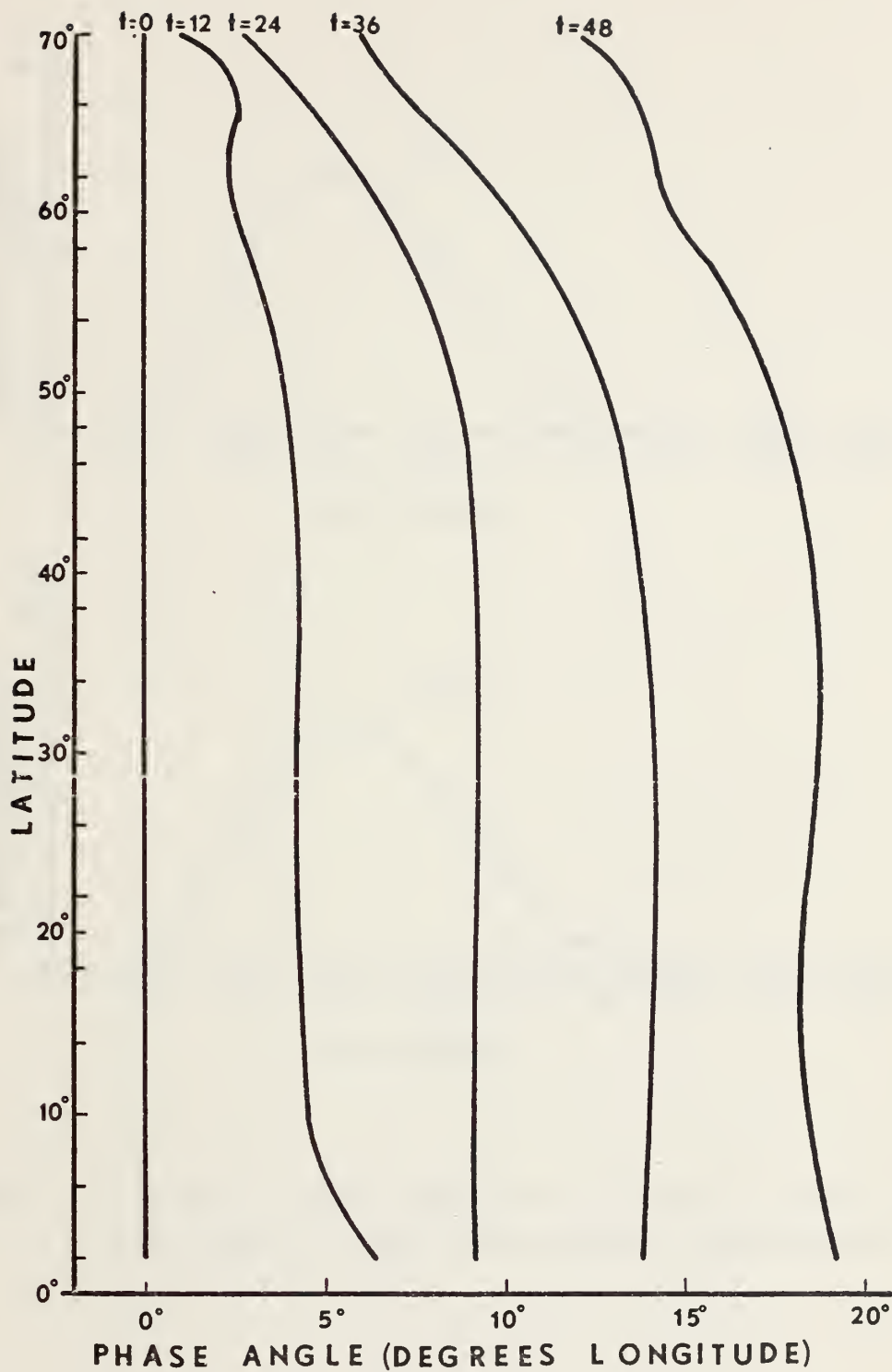


Figure 23. Phase angle (degrees longitude) vs latitude for 46-point N-S grid, wave number 12, phase speed  $10^\circ/\text{day}$  and  $A = 7.0 \times 10^7$ . (Latitudes with zero amplitude are not included and time is given in hours.)



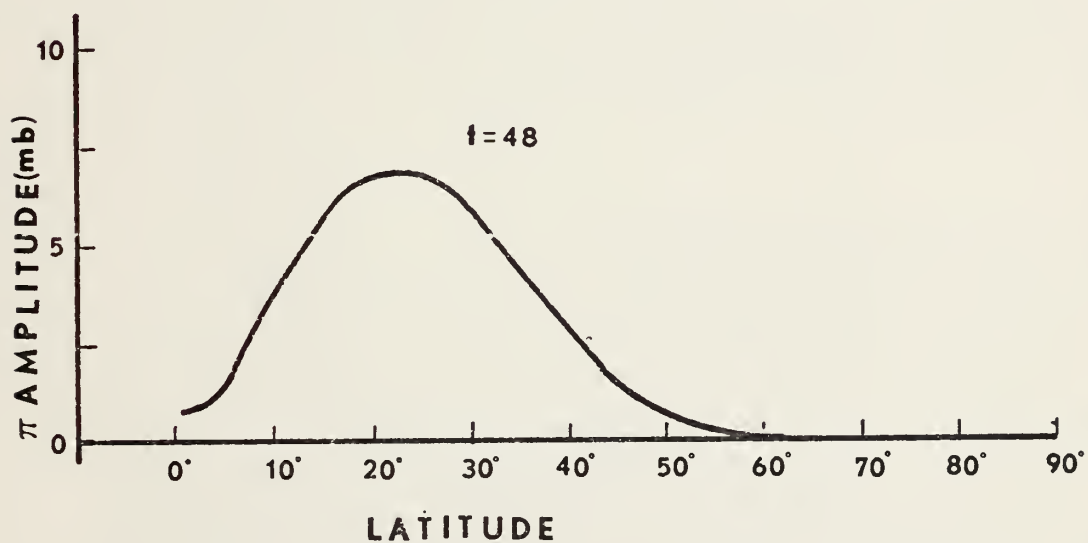
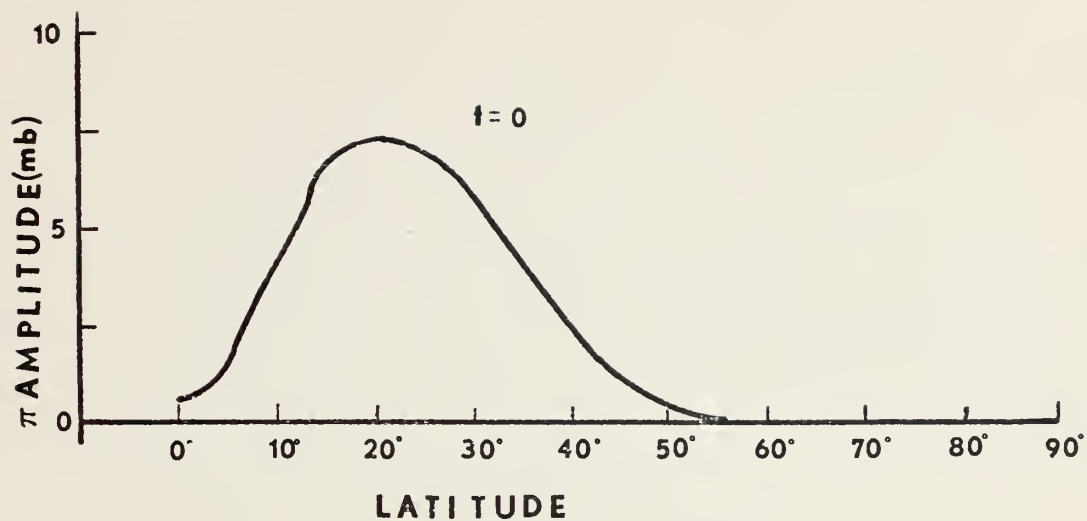


Figure 24. Terrain pressure amplitude vs latitude for initial field and 48-hour forecast, wave number 12, phase speed  $10^\circ/\text{day}$  and  $A = 7.0 \times 10^7$ .





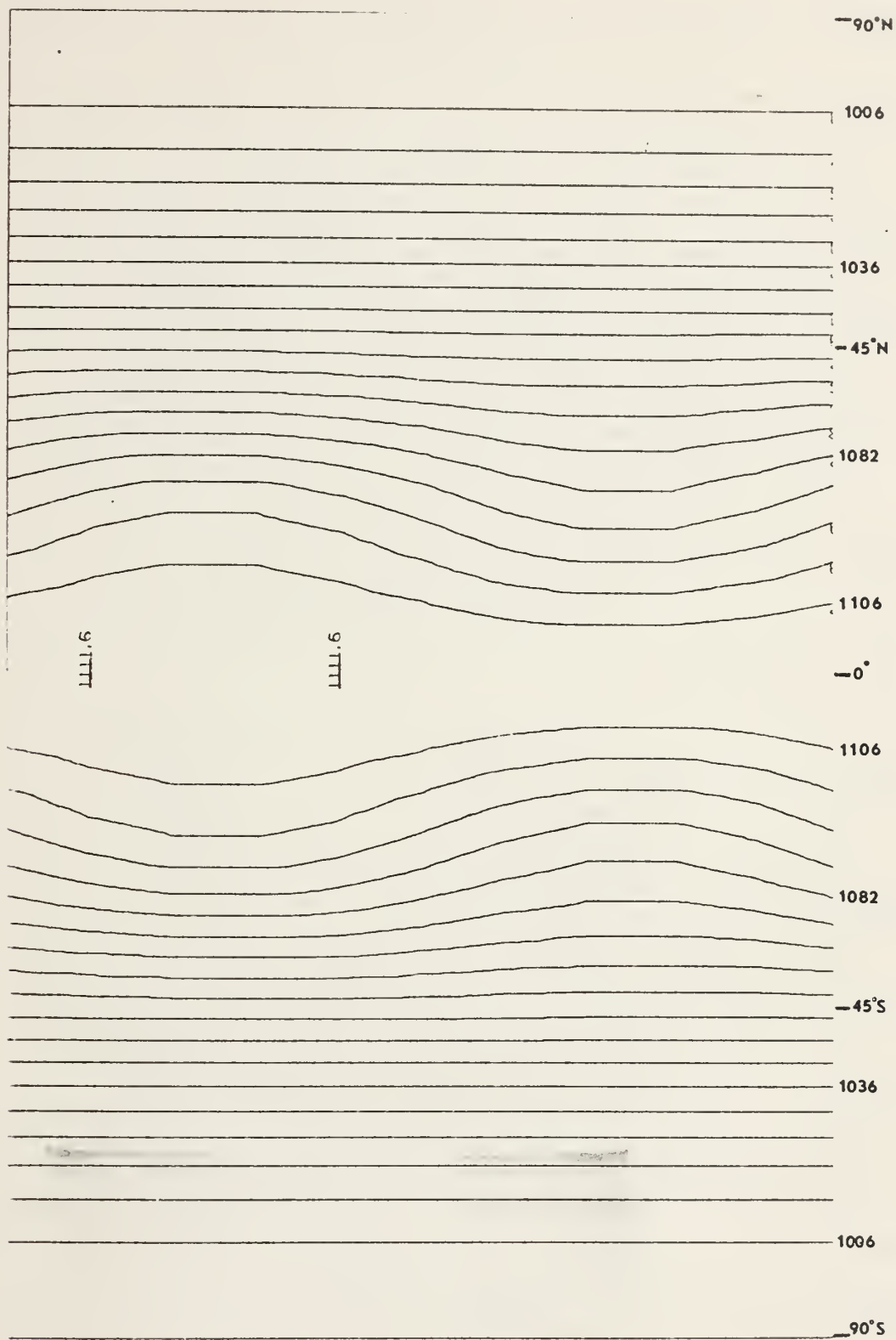


Chart K. Initial surface pressure analysis for 46-point N-S grid, wave number 12, phase speed  $10^\circ/\text{day}$  and  $A = 7.0 \times 10^7$ .



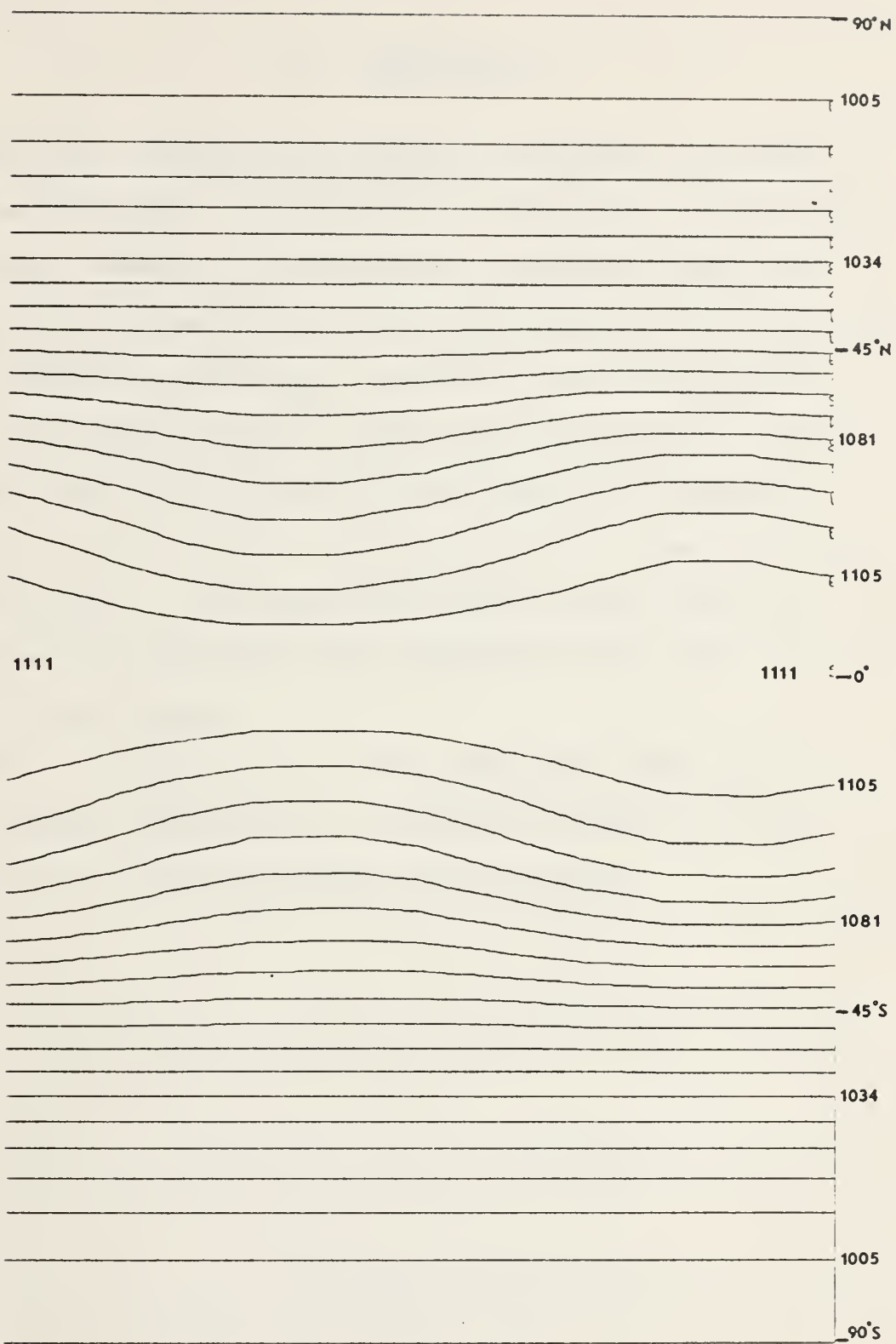


Chart L. 48-hour surface pressure forecast for 46-point N-S grid, wave number 12, phase speed  $10^\circ/\text{day}$  and  $A = 7.0 \times 10^7$ .



## VI. CONCLUSION

The model remained well-behaved throughout all experiments and the phase speeds were less than for the non-divergent model, however, they equaled or exceeded theoretical expectations as described by Williams (1972). The model, as it is presently constructed, appears to have the desired horizontal flexibility as evidenced by the fact that the experiments were carried out with different grid spacings. The vertical flexibility, although built in, was not tested in this report. The simplified nature of the model precluded direct comparison with existing global models such as FNWC's 5-level model.

Future research efforts with this model should most likely include expansion to 5-levels, treatment of cross polar flow and initialization with real data.



## LIST OF REFERENCES

1. Arakawa, A., Design of the UCLA General Circulation Model, Department of Meteorology, University of California, Los Angeles, Technical Report No. 7, 1-89, July 1972.
2. \_\_\_\_\_, and Mintz, Y., The UCLA General Circulation Model, Department of Meteorology, University of California, Los Angeles, Workshop Notes, 25 March-4 April 1974, I-VIII, 1974.
3. Elias, W.E., Numerical Experiments With a Five-Level Global Atmospheric Prediction Model Using a Staggered, Spherical, Sigma Coordinate System, M.S. Thesis, Naval Postgraduate School, Monterey, California, 1973.
4. Gates, W.L., Batten, E.S., Kahle, A.B. and Nelson, A.B., A Documentation of the Mintz-Arakawa Two-Level Atmospheric General Circulation Model, Advanced Research Projects Agency Report R-877-ARPA, December, 1971.
5. Haltiner, G.J., Numerical Weather Prediction, 193-196, Wiley, 1971.
6. \_\_\_\_\_, and Martin, F.L., Dynamical and Physical Meteorology, 52-53, McGraw Hill, 1957.
7. Haurwitz, B., "The Motion of Atmospheric Disturbances on Spherical Earth," J. Marine Research (Sears Foundation), 3, 254-267, 1940.
8. Langlois, W.E. and Kwok, H.C.W., Numerical Simulation of Weather and Climate, Large Scale Scientific Computation Department, IBS Research Laboratory, San Jose, California, 1-54, 74-89, 1969.
9. Maher, D.E., Experiments With a 5-Level Global Primitive Equation Atmospheric Model Using Analytically Determined Fields, M.S. Thesis, Naval Postgraduate School, Monterey, California, 1974.
10. McCollough, J.M., Fourth-Order Differencing in a Five-Level Spherical Sigma Coordinate Global Weather Prediction Model, M.S. Thesis, Naval Postgraduate School, Monterey, California, 1974.
11. Mihok, W.F., Fourth-Order Differencing in a Five-Layer Spherical Sigma Coordinate Global Weather Prediction Model, M.S. Thesis, Naval Postgraduate School, Monterey, California, 1974.





12. Neamtan, S.M., "The Motion of Harmonic Waves in the Atmosphere," J. Meteorology, 3, 53-56, 1946.
13. Phillips, N.A., "Numerical Integration of the Primitive Equation on the Hemisphere," Mon. Wea. Rev., 333-345, 1959.
14. Williams, R.T., Phase Speed Errors With Second and Fourth Order Space Differences with Staggered and Unstaggered Grids, Naval Postgraduate School Report NPS-51Wu72039A, March 1972.
15. Winninghoff, F.J., On the Adjustment Towards a Geostrophic Balance in a Simple Primitive Equation Model with Application to the Problems of Initialization and Objective Analysis, Ph.D. Thesis, Dept. of Meteorology, University of California, Los Angeles, 1968.



# INITIAL DISTRIBUTION LIST

	No. Copies
1. Defense Documentation Center Cameron Station Alexandria, Virginia 22314	2
2. Library, Code 0212 Naval Postgraduate School Monterey, California 93940	2
3. Dr. George J. Haltiner, Code 51Ha Department of Meteorology Naval Postgraduate School Monterey, California 93940	1
4. Dr. Roger T. Williams, Code 51Wu Department of Meteorology Naval Postgraduate School Monterey, California 93940	2
5. LT Anthony V. Monaco NWSED NAF Sigonella FPO, New York 09523	2



Thesis  
M6697  
c.2

Monaco

An atmospheric global  
prediction model using  
a modified Arakawa dif-  
ferencing scheme.

158815

Thesis  
M6697  
c.2

Monaco

An atmospheric global  
prediction model using  
a modified Arakawa dif-  
ferencing scheme.

158815

thesM6697

An atmospheric global prediction model u



3 2768 002 04691 4

DUDLEY KNOX LIBRARY